Simplified Channel Estimation Techniques for OFDM Systems with Realistic Indoor Fading Channels

by

Jake Hwang

A thesis
presented to the University of Waterloo
in fulfillment of the
thesis requirement for the degree of
Master of Applied Science
in
Electrical and Computer Engineering

Waterloo, Ontario, Canada, 2009

I hereby declare that I am the sole author of this thesis. This is a true copy of the thesis, including any required final revisions, as accepted by my examiners.

I understand that my thesis may be made electronically available to the public.

Jake Hwang

Abstract

This dissertation deals with the channel estimation techniques for orthogonal frequency division multiplexing (OFDM) systems such as in IEEE 802.11. Although there has been a great amount of research in this area, characterization of typical wireless indoor environments and design of channel estimation schemes that are both robust and practical for such channel conditions have not been thoroughly investigated. It is well known that the minimum mean-square-error (MMSE) estimator provides the best mean-square-error (MSE) performance given *a priori* knowledge of channel statistics and operating signal-to-noise ratio (SNR). However, the channel statistics are usually unknown and the MMSE estimator has too much computational complexity to be realized in practical systems. In this work, we propose two simple channel estimation techniques: one that is based on modifying the channel correlation matrix from the MMSE estimator and the other one with *averaging window* based on the LS estimates. We also study the characteristics of several realistic indoor channel models that are of potential use for wireless local area networks (LANs). The first method, namely MMSE-exponential-Rhh, does not depend heavily on the channel statistics and yet offer performance improvement compared to that of the LS estimator. The simulation results also show that the second method, namely averaging window (AW) estimator, provides the best performance at moderate SNR range.

Acknowledgments

I would like to thank my supervisor, Prof. Amir K. Khandani, for his valuable guidance and support throughout the course of my graduate studies. His passion towards research and care for his student have made this work possible. I would like to thank my readers, Prof. Boumaiza and Prof. Safavi, for their valuable reviews, insights, and suggestions. I would also like to thank my colleagues at CST lab for their insightful discussions and supports.

I would like to thank my family for their unconditional love and belief in me. Lastly, my special thank goes to the love of my life, Hyaewon Jeon. Without her love, I would have not been where I am.

Contents

List of Figures

List of Tables

Chapter 1

Introduction

Multimedia wireless services require high data-rate transmission over mobile radio channels. Orthogonal Frequency Division Multiplexing (OFDM) is widely considered as a promising choice for future wireless communications systems due to its high-data-rate transmission capability with high bandwidth efficiency. In OFDM, the entire channel is divided into many narrow subchannels, converting a frequency-selective channel into a collection of frequency-flat channels. Moreover, intersymbol interference (ISI) is avoided by the use of cyclic prefix (CP), which is achieved by extending an OFDM symbol with some portion of its head or tail [16]. In fact, OFDM has been adopted in digital audio broadcasting (DAB), digital video broadcasting (DVB), digital subscriber line (DSL), and wireless local area network (WLAN) standards such as the IEEE 802.11a/b/g/n [1–4]. It has also been adopted for wireless broadband access standards such as the IEEE 802.16e [5], and as the core technique for the fourth-generation (4G) wireless mobile Communications [26].

To eliminate the need for channel estimation and tracking, differential phase-shift keying (DPSK) can be used in OFDM systems. However, this results in a 3 dB loss in signal-

to-noise ratio (SNR) compared with coherent demodulation such as phase-shift keying (PSK) [37]. The performance of OFDM systems can be improved by allowing for coherent demodulation when an accurate channel estimation technique is used.

1.1 Channel Estimation in OFDM Systems

Channel estimation techniques for OFDM systems can be grouped into two categories: blind and non-blind. The blind channel estimation method exploits the statistical behaviour of the received signals, while the non-blind channel estimation method utilizes some or all portions of the transmitted signals, i.e., pilot tones or training sequences, which are available to the receiver to be used for the channel estimation.

The main advantage of the blind channel estimation is the possible elimination of training sequences, which decrease the system bandwidth efficiency [18, 45]. Additionally, due to the time-varying nature of the channel in some wireless applications, the training sequence needs to be transmitted periodically, causing further loss of channel throughput. Due to these reasons, reducing the number of training symbols becomes a major concern, and the blind channel estimation algorithms have received considerable attention [18]. There are several types of blind channel estimation techniques found in literature. For example, the subspace-based algorithms using redundant linear precoding are considered in [40, 54] and nonredundant linear precoding in [6, 36]. In these methods, a linear block precoder is applied at the transmitter and the channel information is extracted by exploiting the covariance matrix of the received signals. Other subspace-based blind channel estimators make use of the cyclostationarity inherent in OFDM signal due to CP [11, 15, 19, 33, 51]. Specifically, the authors in [19] proposed a method based on the cyclostationarity property

of the time-varying correlation of the received data samples caused by the CP insertion at the transmitter. Cai *et al.* [11], on the other hand, developed a noise subspace method by utilizing the time-invariant correlation of the received data vector. Other than the use of CP, the subspace-based blind channel estimation using virtual carriers in OFDM symbols is also proposed in [29]. Although these blind channel estimation techniques may be a desirable approach as they do not require training or pilot signals to increase the system bandwidth and the channel throughput, they require, however, a large amount of data in order to make a reliable stochastic estimation. Therefore, they suffer from high computational complexity and severe performance degradation in fast fading channel [8, 50, 53].

On the other hand, the non-blind channel estimation can be performed by either inserting pilot tones into all of the subcarriers of OFDM symbols with a specific period or inserting pilot tones into some of the subcarriers for each OFDM symbol [39]. In the first case, an OFDM symbol with pilot tones in all the subcarriers is often called a training sequence and this type of pilot arrangement is referred to as *block-type* pilot arrangement. Block-type channel estimation is usually developed under the assumption of slow fading channel, where the channel is assumed to be constant over one or more OFDM symbol periods. The channel estimation for this block-type pilot arrangement can be based on Least Square (LS) or Minimum Mean-Square Error (MMSE) [22, 34, 52]. It is well known that the MMSE estimator has good performance but suffers from a high computational complexity. On the other hand, the LS estimator has low complexity, but its performance is not as good as that of the MMSE estimator. In [22], the MMSE estimate has been shown to give up to 4 dB gain in SNR over the LS estimate for the same mean square error (MSE) of the channel estimation. To reduce the complexity of the MMSE estimator,

Edfors *et al.* [34] applied the theory of optimal rank-reduction to linear MMSE estimator by using the singular value decomposition (SVD) [41] and the frequency correlation of the channel.

In the latter case of the non-blind channel estimation, the pilot tones are multiplexed with the data within an OFDM symbol and it is referred to as *comb-type* pilot arrangement. The comb-type channel estimation is performed to satisfy the need for the channel equalization or tracking in fast fading scenario, where the channel changes even in one OFDM period. The main idea in comb-type channel estimation is to first estimate the channel conditions at the pilot subcarriers and then estimate the channel at the data subcarriers by means of interpolation. The estimation of the channel at the pilot subcarriers can be based on LS, MMSE or Least Mean-Square (LMS). Once channel coefficients are estimated at the pilot subcarriers, they are *tracked* by using adaptive Wiener filters such as Normalized Least Mean-Square (NLMS) and Recursive Least Square (RLS) [14]. In these methods, the channel impulse response (CIR) taps are updated based on the cost functions defined for NLMS and RLS. Although NLMS is less complex and less accurate compared to RLS, care must be taken in RLS algorithm for oversampled systems, as the performance can be faulty due to implicit matrix inversion needed during update operation [44]. In [20, 39], a variety of interpolation schemes are investigated and compared, including linear interpolation, second-order interpolation, low-pass interpolation, spline cubic interpolation, and time domain interpolation. The authors showed that the performance among these interpolation techniques range from the best to the worst, as follows: low-pass, spline cubic, time domain, second-order and linear interpolation. Regardless of the use of interpolation scheme, the performance of the channel estimation using comb-type pilot arrangement is

directly influenced by the number and/or locations of pilot subcarriers used for the initial estimation [35]. In other words, the number of pilot subcarriers needs to be high enough such that the frequency spacing between the pilot subcarriers is smaller than the channel coherence bandwidth in order to obtain a reliable estimation. Therefore, the comb-type channel estimation may not be suitable for some applications, such as the wireless LANs [1–4] where the number of pilot tones is too small compared to the number of data tones and their locations are fixed.

Another type of non-blind channel estimation technique is called a Decision Directed Channel Estimation (DDCE). The main idea behind DDCE is to use the channel estimation of a previous OFDM symbol for the data detection of the current estimation, and thereafter using the newly detected data for the estimation of the current channel [27, 32]. Once the data at the subcarriers is detected, any methods described above can be used to estimate the current channel. The major benefit of the DDCE scheme is that in contrast to purely *pilot assisted* channel estimation methods, both the pilot symbols as well as all the information symbols are utilized for channel estimation [9]. On the other hand, the DDCE inherently introduces two basic problems: the use of outdated channel estimates, and the assumption of correct data detection. The use of outdated channel estimates does not pose a serious issue when the channel is varying very slowly. However, when the channel starts varying faster, then the outdated channel estimates for the previous OFDM symbol are no longer valid for the use of the data detection in the current OFDM symbol. Hence, the error in the channel estimation and data detection build up to make the system performance unacceptable [12]. In addition, this error propagation can be also amplified by any discrepancies in the system, which limits its use in practical systems.

1.2 Contributions of Thesis

This thesis focuses on the non-blind channel estimation techniques that are based on the block-type pilot arrangement. Once we establish reliable and practical channel estimation schemes for this type of pilot arrangement, we expect that our proposed schemes can be simply applied to the systems with comb-type pilot arrangement (or DDCE) and use the interpolation methods discussed previously. A second objective of this thesis is to investigate the characteristics of the typical indoor environments in which actual wireless network such as WLAN is deployed. Having understood the behaviour of radio propagation in such environments, we then present the performance analysis of our proposed techniques.

1.3 Organization of Thesis

The remainder of this thesis is organized as follows. In Chapter 2, the OFDM system model under investigation is described. In Chapter 3, we present the LS and MMSE estimator, along with our proposed methods. We also remark on some interesting aspects of the estimators. In Chapter 4, we investigate the realistic indoor channel models and analyze the mean-square-error (MSE) and bit-error-rate (BER) performance of the proposed methods. Design considerations and trade offs are also discussed in this chapter. Lastly, conclusions and future research are presented in Chapter 5.

Chapter 2

OFDM System Description

The basic idea underlying OFDM systems is the division of the available frequency spectrum into several subcarriers, converting a frequency-selective channel into a parallel collection of frequency flat subchannels [42]. To obtain a high spectral efficiency, the signal spectra corresponding to the different subcarriers overlap in frequency, and yet they have the minimum frequency separation to maintain orthogonality of their corresponding time domain waveforms [17]. The use of a CP both preserves the orthogonality of the tones and eliminates ISI between consecutive OFDM symbols.

A block diagram of a baseband OFDM system is shown in Figure 2.1. After the information bits are grouped, coded and modulated, they are fed into N-point inverse fast Fourier transform (IFFT) to obtain the time domain OFDM symbols, i.e.,

$$x_n = IFFT_N\{X_k\} \tag{2.1}$$

$$= \sum_{k=0}^{N-1} X_k e^{j2\pi nk/N}, \quad 0 \le n, k \le N-1 \tag{2.2}$$

, where n is the time domain sampling index, X_k is the data at kth subcarrier, and N is the total number of subcarriers. Following IFFT block, a cyclic extension of time length, T_G, chosen to be larger than the expected maximum delay spread of the channel [28], is inserted to avoid intersymbol and intercarrier interferences.

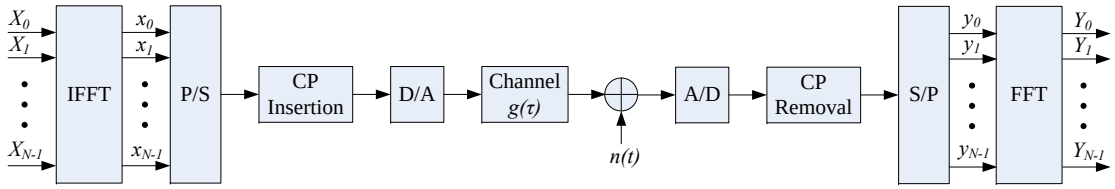

Figure 2.1: Baseband OFDM

The digital-to-analog (D/A) converter contains low-pass filters with bandwidth $1/T_s$, where T_s is the sampling interval or an OFDM symbol period. The channel is modeled as an impulse response, $g(\tau)$, followed by the complex additive white Gaussian noise (AWGN), $n(t)$ [43].

$$g(\tau) = \sum_{m=0}^{M-1} \alpha_m \delta(\tau - \tau_m T_s) \tag{2.3}$$

, where M is the number of multipaths, α_m is the mth path gain in complex, and τ_m is the corresponding path delay. At the receiver, after passing through the analog-to-digital (A/D) and removing CP, the N-point FFT is used to transform the data back to frequency domain. Finally, the information bits are obtained after the channel equalization/decoding, and demodulation.

Under the assumption that the use of a CP preserves the orthogonality of the tones and the entire impulse response lies inside the guard interval, i.e., $0 \leq \tau_m T_s \leq T_G$ [17, 22], we can describe the received signals as

$$\boldsymbol{Y} = FFT_N \left\{ IFFT_N \left\{ \mathbf{X} \right\} \otimes \boldsymbol{g} + \tilde{\boldsymbol{n}} \right\} \tag{2.4}$$

, where $\boldsymbol{Y} = [Y_0 \; Y_1 \; \cdots \; Y_{N-1}]^T$ is the received vector, $\mathbf{X} = [X_0 \; X_1 \; \cdots \; X_{N-1}]^T$ is a vector of the transmitted signal, and $\boldsymbol{g} = [g_0 \; g_1 \; \cdots \; g_{N-1}]^T$ and $\tilde{\boldsymbol{n}} = [\tilde{n}_0 \; \tilde{n}_1 \; \cdots \tilde{n}_{N-1}]^T$ are the sampled frequency response of $g(\tau)$ and AWGN, respectively. Note that both $\boldsymbol{Y}$ and $\mathbf{X}$ are frequency domain data.

In fact, the expression in equation (2.4) is equivalent to a transmission of data over a set of parallel Gaussian channels [34], as shown in Figure 2.2.

Therefore, the system described by equation (2.4) can be written as

$$\boldsymbol{Y} = \boldsymbol{X}\boldsymbol{F}\boldsymbol{g} + \boldsymbol{F}\tilde{\boldsymbol{n}} \tag{2.5}$$

, where $\boldsymbol{X}$ is a diagonal matrix containing the elements of $\mathbf{X}$ in equation (2.4), and

$$\boldsymbol{F} = \begin{bmatrix} W_N^{00} & \cdots & W_N^{0(N-1)} \\ \vdots & \ddots & \vdots \\ W_N^{(N-1)0} & \cdots & W_N^{(N-1)(N-1)} \end{bmatrix} \tag{2.6}$$

is the FFT matrix with

$$W_N^{nk} = \frac{1}{\sqrt{N}} e^{-j2\pi \frac{nk}{N}}. \tag{2.7}$$

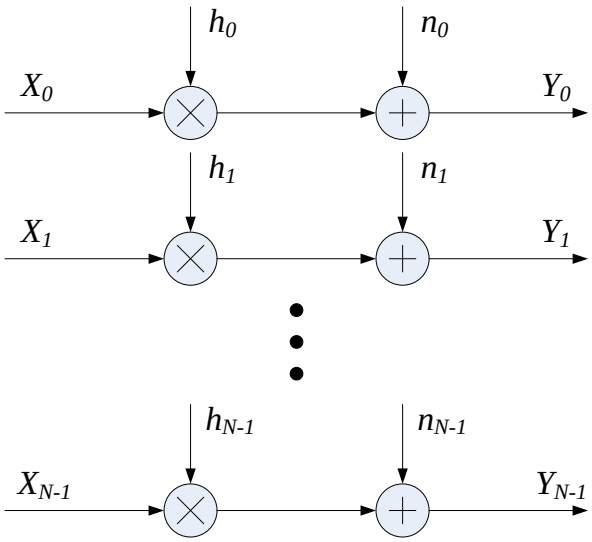

Figure 2.2: The OFDM system, modeled as parallel Gaussian channels

Also, let $\boldsymbol{h} = FFT_N\{\boldsymbol{g}\} = \boldsymbol{F}\boldsymbol{g}$ and $\boldsymbol{n} = FFT_N\{\tilde{\boldsymbol{n}}\} = \boldsymbol{F}\tilde{\boldsymbol{n}}$. Thus, equation (2.5) now becomes

$$\boldsymbol{Y} = \boldsymbol{X}\boldsymbol{h} + \boldsymbol{n}. \tag{2.8}$$

In this work, we assume that the noise $\boldsymbol{n}$ is a vector of independent identically distributed (i.i.d.) complex zero-mean Gaussian noise with variance σ_n^2. We also assume that $\boldsymbol{n}$ is uncorrelated with the channel $\boldsymbol{h}$.

Chapter 3

Channel Estimation Techniques

As discussed in Section 1.1, there are two different ways of arranging pilot tones in OFDM transmission: block-type pilot arrangement and comb-type pilot arrangement, as shown in Figure 3.1.

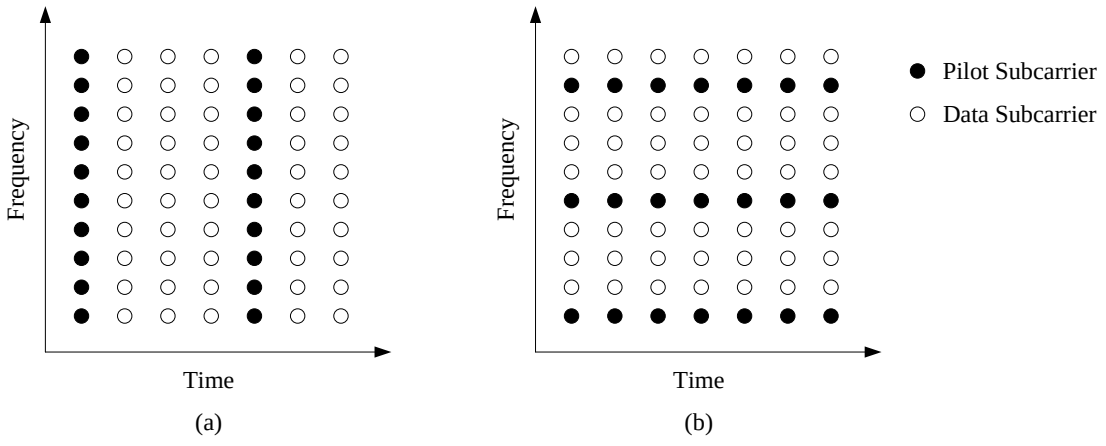

Figure 3.1: Two different types of pilot arrangement: (a) block-type pilot arrangement and (b) comb-type pilot arrangement

For the channel estimation based on block-type pilot arrangement, the spacing between consecutive training sequences needs to be determined carefully. When the channel varies across OFDM symbols in time, the training sequence must be inserted at a ratio that is determined by the coherence time or Doppler spread. In [38], a quantitative expression, based on the Nyquist sampling theorem for the maximum spacing of training sequence in time, $N_{t,max}$, is given by

$$N_{t,max} \leq \frac{1}{2nf_{D,max}T_s} \tag{3.1}$$

, where n is the oversampling factor, $f_{D,max}$, is the maximum Doppler spread, and T_s is the OFDM symbol duration. Therefore, if the training sequence is inserted at the start of the packet or block similar to those in WLAN, the packet length should be smaller than $N_{t,max}T_s$ in time.

Similarly, the spacing of pilot tones within an OFDM symbol, in the case of comb-type channel estimation, should also be small enough so that the variations of the channel in frequency can be captured. That is,

$$N_{f,max} \leq \frac{1}{n\tau_{max}\Delta f} \tag{3.2}$$

, where τ_{max} is the maximum delay spread and Δf is the subcarrier spacing in OFDM symbol. Here, the pilot spacing should be smaller than $N_{f,max}\Delta f$ in frequency or simply $N_{f,max}$ subcarrier spacings in order to be able to perform an interpolation.

Regardless of which pilot arrangement scheme is used for the non-blind channel estimation, the basic channel estimation technique is the same for both schemes. That is, the comb-type pilot channel estimation can be treated as a special case of the block-type

pilot channel estimation, where the channel estimation technique is performed only at the pilot subcarriers, followed by the interpolation at the data subcarriers. In this work, we only consider the frequency domain initial channel estimation techniques based on the block-type pilot arrangement, assuming equation (3.1) is satisfied.

In this chapter, the LS estimation technique is presented as it is needed by many estimation techniques as an initial estimation, followed by the MMSE estimator. Then, the modified MMSE estimator is proposed in an attempt to reduce the computational complexity and eliminate the need for *a priori* knowledge of the channel statistics. We also propose another simple and effective channel estimator which is based on the LS estimate.

3.1 Least-Square Estimator

From equation (2.8), the LS estimator minimizes the following cost function [47]

$$\min_{\hat{\boldsymbol{h}}} (\boldsymbol{Y} - \boldsymbol{X}\hat{\boldsymbol{h}})^H (\boldsymbol{Y} - \boldsymbol{X}\hat{\boldsymbol{h}}) \tag{3.3}$$

, where $[\cdot]^H$ is the Hermitian (conjugate) transpose operator. Then, the LS estimation of $\boldsymbol{h}$ is given by

$$\hat{\boldsymbol{h}}_{LS} = \frac{\boldsymbol{Y}}{\boldsymbol{X}} = \left[\frac{Y_k}{X_k}\right]^T \tag{3.4}$$

, where $[\cdot]^T$ is the transpose operator and $k = 0, 1, \cdots, N-1$. This LS estimator is equivalent to what is also referred to as the *zero-forcing* estimator [22, 30] since it can also be obtained from the time domain LS estimator with no assumption on the number of CIR

taps or length. That is,

$$\hat{\boldsymbol{h}}_{LS} = \boldsymbol{F}\boldsymbol{Q}_{LS}\boldsymbol{F}^{\boldsymbol{H}}\boldsymbol{X}^{\boldsymbol{H}}\boldsymbol{Y} \tag{3.5}$$

, where

$$\boldsymbol{Q}_{LS} = \left(\boldsymbol{F}^{\boldsymbol{H}}\boldsymbol{X}^{\boldsymbol{H}}\boldsymbol{X}\boldsymbol{F}\right)^{-1}. \tag{3.6}$$

Note that this simple LS estimator does not exploit the correlation of channel across subcarriers in frequency and across the OFDM symbols in time. Without using any knowledge of the statistics of the channel, the LS estimator can be calculated with very low complexity, but it has a high mean-square error since it does not take into account of the effect of noise on the signal.

3.2 Minimum Mean-Square Error Estimator

The minimum mean-square error is widely used in the OFDM channel estimation since it is optimum in terms of mean square error (MSE) in the presence of AWGN [7]. In fact, it is observed in [35] that many channel estimation techniques are indeed a subset of MMSE channel estimation technique. The MMSE estimator employs the second-order statistics of the channel, channel correlation function, and the operating SNR.

Let us define $\boldsymbol{R}_{\boldsymbol{gg}}$, $\boldsymbol{R}_{\boldsymbol{hh}}$, and $\boldsymbol{R}_{\boldsymbol{YY}}$ as the autocovariance matrix of $\boldsymbol{g}$, $\boldsymbol{h}$, and $\boldsymbol{Y}$, respectively. We also define $\boldsymbol{R}_{\boldsymbol{gY}}$ as the crosscovariance matrix between $\boldsymbol{g}$ and $\boldsymbol{Y}$. Assuming the channel vector, $\boldsymbol{h}$, and the noise vector, $\boldsymbol{n}$, are uncorrelated, we derive that

$$\boldsymbol{R}_{\boldsymbol{hh}} = E\left\{\boldsymbol{H}\boldsymbol{H}^{H}\right\} = E\left\{(\boldsymbol{F}\boldsymbol{g})(\boldsymbol{F}\boldsymbol{g})^{H}\right\} = \boldsymbol{F}\boldsymbol{R}_{\boldsymbol{gg}}\boldsymbol{F}^{H}, \tag{3.7}$$

$$\boldsymbol{R_{gY}} = E\left\{\boldsymbol{gY}^H\right\} = E\left\{\boldsymbol{g}(\boldsymbol{XFg}+\boldsymbol{n})^H\right\} = \boldsymbol{R_{gg}F}^H\boldsymbol{X}^H \tag{3.8}$$

, and

$$\boldsymbol{R_{YY}} = E\left\{\boldsymbol{YY}^H\right\} = \boldsymbol{XFR_{gg}F}^H\boldsymbol{X}^H + \sigma_{\boldsymbol{n}}^2\boldsymbol{I}_N \tag{3.9}$$

where $\sigma_{\boldsymbol{n}}^2$ is the noise variance, $E\left\{|\boldsymbol{n}|^2\right\}$, and $\boldsymbol{I}_N$ is the $N \times N$ Identity matrix. Assuming the channel correlation matrix, $\boldsymbol{R_{hh}}$, and the operating SNR, $\sigma_{\boldsymbol{n}}^2$, are known at the receiver, the MMSE estimator of $\boldsymbol{g}$ is given by [22, 34, 39, 49]

$$\hat{\boldsymbol{g}}_{MMSE} = \boldsymbol{R_{gY}R_{YY}^{-1}Y}. \tag{3.10}$$

Finally, combining the above equations, the frequency domain MMSE estimator can be calculated by

$$\begin{aligned}
\hat{\boldsymbol{h}}_{MMSE} &= \boldsymbol{F}\hat{\boldsymbol{g}}_{MMSE} \\
&= \boldsymbol{F}[(\boldsymbol{F}^H\boldsymbol{X}^H)^{-1}\boldsymbol{R_{gg}^{-1}}\sigma_{\boldsymbol{n}}^2 + \boldsymbol{XF}]^{-1}\boldsymbol{Y} \\
&= \boldsymbol{FR_{gg}}[(\boldsymbol{F}^H\boldsymbol{X}^H\boldsymbol{XF})^{-1}\sigma_{\boldsymbol{n}}^2 + \boldsymbol{R_{gg}}]\boldsymbol{F^{-1}}\hat{\boldsymbol{h}}_{LS} \\
&= \boldsymbol{R_{hh}}[\boldsymbol{R_{hh}} + \sigma_{\boldsymbol{n}}^2(\boldsymbol{XX}^H)^{-1}]^{-1}\hat{\boldsymbol{h}}_{LS}.
\end{aligned} \tag{3.11}$$

The above MMSE estimator yields much better performance than LS estimator, especially under the low SNR scenarios. However, a major drawback of the MMSE estimator is its high computational complexity, since the matrix inversion of size $N \times N$ is needed each time data in $\boldsymbol{X}$ changes.

Another drawback of this estimator is that it requires one to know the correlation of the channel and the operating SNR in order to minimize the MSE between the transmitted and

received signals. However, in wireless links, the channel statistics depend on the particular environment, for example, indoor or outdoor, Line-Of-Sight (LOS) or Non-Line-Of-Sight (NLOS), and changes with time [52]. Therefore, MMSE estimator may not be feasible in a practical system.

3.3 Proposed Methods

As discussed in the previous section, the channel estimation based on MMSE is the best estimator in terms of MSE performance at a cost of high computational complexity. In this section, we propose two different channel estimation techniques with low complexity and robustness against channel conditions.

3.3.1 Modified MMSE Method

In addition to a high computational complexity, the MMSE estimator requires *a priori* knowledge of the second-order statistics of the channel condition, i.e., the channel correlation function across the frequency tones. Such information is embedded in the channel correlation matrix $\boldsymbol{R_{hh}}$ from equation (3.11), which plays a critical role in reducing noise that is added on top of the LS estimation.

First, we examine the expression of $\boldsymbol{R_{hh}}$, proposed by Edfors *et al.* [34]:

$$\boldsymbol{R_{hh}} = E\left\{\boldsymbol{h}\boldsymbol{h}^H\right\} = [r_{m,n}] \tag{3.12}$$

and

$$r_{m,n} = \frac{1 - e^{-\tau_{max}((1/\tau_{rms})+2\pi j(m-n)/N)}}{\tau_{rms}(1 - e^{-(\tau_{max}/\tau_{rms})})(\frac{1}{\tau_{rms}} + j2\pi\frac{m-n}{N})} \tag{3.13}$$

, where $m, n = 0, 1, \cdots, N-1$, τ_{rms} is a root-mean square (rms) delay spread, and τ_{max} is the maximum delay spread. Here, it is assumed that an exponentially decaying power-delay profile $\theta(\tau_m) = Ce^{-\tau_m/\tau_{rms}}$ and delays τ_m from equation (2.3) are uniformly and independently distributed over the length of the maximum delay spread.

In practice, however, the true channel information and the corresponding delay spread values are not known. Hence, as pointed out in [52], it is not robust to design a MMSE estimator that *tightly* matches the channel statistics. It is also computationally very heavy that it is not feasible to update $\boldsymbol{R_{hh}}$ every time the channel changes. Therefore, we propose a different approach of modeling the channel correlation matrix, which is described in the following section.

Exponential $\boldsymbol{R_{hh}}$ Model

Here, we adopt a concept of first-order finite-state Markov chain [10, 13] to represent the channel correlation matrix $\boldsymbol{R_{hh}}$, such that it eliminates the need for *a priori* knowledge of the channel (rms/maximum delay spread and assumptions imposed on multipath delays) and reduces the computational complexity, while it closely follows the behaviour of the *true* channel correlation matrix. In general, a first-order Markov chain is widely used to represent a slowly time-varying channel and defined by its initial-state occupancy probabilities and its transition probabilities [25]. As stated in [48], the first-order Markovian assumption implies that, given the information on the state immediately preceding the current one, any other previous state should be independent of the current state. In our case, we assume that the channel correlation matrix depends only on the correlation of two consecutive channel attenuations (having a memory of 1), with such correlation parameter

being analogous to *state* in Markovian model. The correlation parameter ρ is modeled as a magnitude of the channel autocorrelation function where the distance between the tones is 1. For example,

$$\rho = \left| E\left\{ h_{p+q} h_p^* \right\} \right| = \left| \sum_{p=0}^{N-q-1} h_{p+q} h_p^* \right|, \qquad q = 1. \tag{3.14}$$

Then, a new channel correlation matrix $\tilde{\boldsymbol{R}}_{\boldsymbol{hh}}$ is constructed such that its elements are the exponential series of ρ. That is,

$$\begin{aligned} \Re\left\{\tilde{r}_{m,n}\right\} &= \left[\rho^{|m-n|}\right] \\ &= \begin{bmatrix} 1 & \rho & \rho^2 & \cdots & \rho^{N-1} \\ \rho & 1 & \rho & \cdots & \rho^{N-2} \\ \vdots & & \vdots & & \vdots \\ \rho^{N-1} & \rho^{N-2} & \rho^{N-3} & \cdots & 1 \end{bmatrix} \end{aligned} \tag{3.15}$$

and

$$\begin{aligned} \Im\left\{\tilde{r}_{m,n}\right\} &= \begin{cases} \left[1-\rho^{|m-n|}\right], & m \le n \\ \left[-\left(1-\rho^{|m-n|}\right)\right], & otherwise \end{cases} \\ &= \begin{bmatrix} 0 & 1-\rho & 1-\rho^2 & \cdots & 1-\rho^{N-1} \\ -(1-\rho) & 0 & 1-\rho & \cdots & 1-\rho^{N-2} \\ \vdots & & \vdots & & \vdots \\ -(1-\rho^{N-1}) & -(1-\rho^{N-2}) & -(1-\rho^{N-3}) & \cdots & 0 \end{bmatrix} \end{aligned} \tag{3.16}$$

, where $m, n = 0, 1, \cdots, N-1$. Combining equation (3.15) and equation (3.16), we have

$\tilde{\boldsymbol{R}}_{\boldsymbol{hh}}$ as a form of symmetric or Hermitian Toeplitz matrix, same as $\boldsymbol{R}_{\boldsymbol{hh}}$. In this modification, we aim to *remodel* $\boldsymbol{R}_{\boldsymbol{hh}}$ using properties of first-order Markov chain, such that the new channel correlation matrix $\tilde{\boldsymbol{R}}_{\boldsymbol{hh}}$ has similar properties as the true channel correlation matrix $\boldsymbol{R}_{\boldsymbol{hh}}$, which is a correlation between the channel attenuations h_m and h_n, not the data subcarriers X_m and X_n. The analytical comparison between $\boldsymbol{R}_{\boldsymbol{hh}}$ and $\tilde{\boldsymbol{R}}_{\boldsymbol{hh}}$ is discussed in the following section.

Analysis of Channel Correlation Matrices

To illustrate the characteristics of the channel correlation matrices, $\boldsymbol{R}_{\boldsymbol{hh}}$ and $\tilde{\boldsymbol{R}}_{\boldsymbol{hh}}$, let us assume a system with $N = 64$ tones and a channel with $\tau_{rms} = 15ns$ and $\tau_{max} = 80ns$. Since they are both Hermitian Toeplitz matrices, we will consider the elements on the first row, which represent the correlation of the channel attenuation at the first tone $m = 1$ against the channel attenuations at the rest of the tones. As can be seen from Figure 3.2, the correlation decreases as the distance of the tones $m - n$ increases for $\boldsymbol{R}_{\boldsymbol{hh}}$ (labeled as Edfors Rhh).

For $\tilde{\boldsymbol{R}}_{\boldsymbol{hh}}$ (labeled as Exponential Rhh), it behaves similarly to that of $\boldsymbol{R}_{\boldsymbol{hh}}$ as the correlation of channel attenuations decreases while the distance of the tones increases. However, its correlation curve levels out for the second half of the tones. This can be interpreted as the channel correlation being more or less the same for the tones with a distance larger than $N/2$.

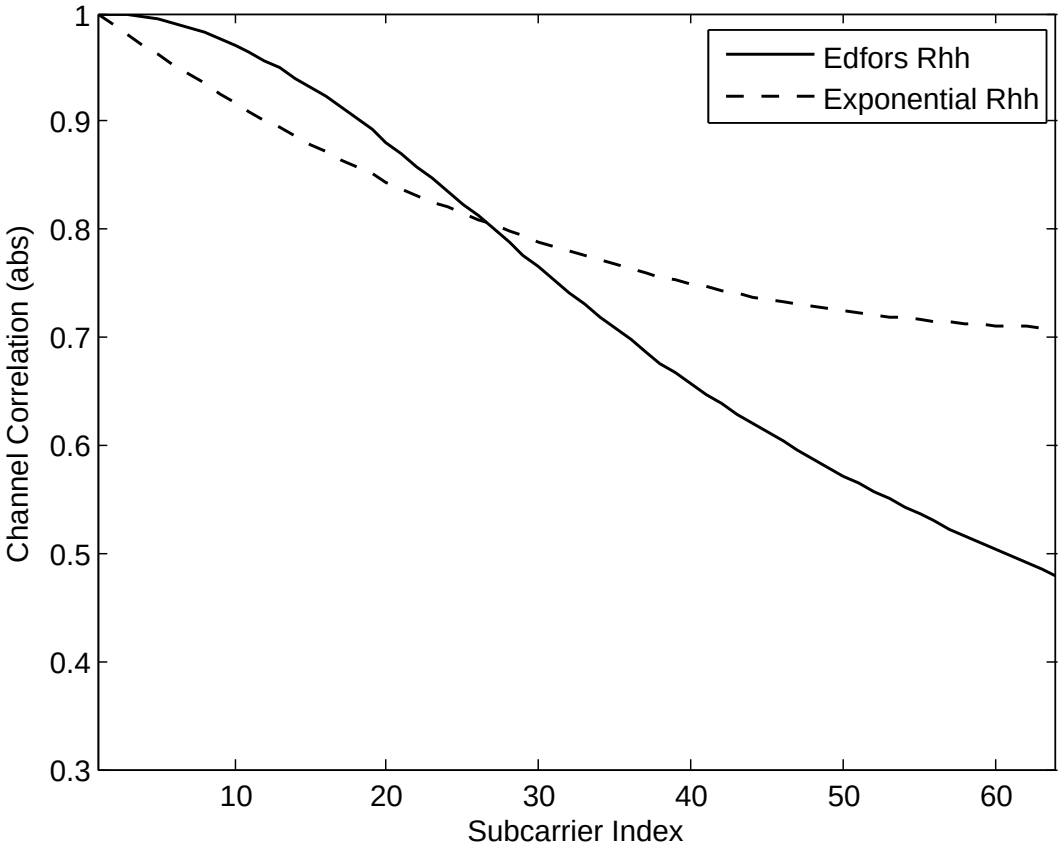

Figure 3.2: The channel correlation of the attenuation at $m = 1$ with the rest of attenuations in case where $N = 64$, $\tau_{rms} = 15ns$, $\tau_{max} = 80ns$, and $\rho = 0.98$

3.3.2 Averaging Window Method

We propose another channel estimation technique, which demonstrates a low computational complexity and effectively reduces the noise that comes with the LS estimate. The goal here is to reduce the effect of noise, especially when the channel SNR is low, by averaging a few LS estimates around the tone of interest. For example, if the averaging window

size is M, the final estimate at the kth subcarrier can be expressed as

$$\hat{h}_{AW;k} = \frac{1}{M} \sum_{i} \hat{h}_{LS;i} \ , \quad k - \left\lfloor \frac{M}{2} \right\rfloor \leq i \leq k + \left\lfloor \frac{M}{2} \right\rfloor \tag{3.17}$$

, where $\hat{h}_{LS;i}$ is the LS estimate at the ith subcarrier. This method can be viewed as an averaging window *sliding* across the tones that are circularly arranged. The size of averaging window, M, should be carefully selected such that the Averaging Window (AW) method minimizes the MSE for a given operating SNR, i.e., M should be large in the low SNR range and small in the high SNR range. It should also depend on how much the channel fluctuates across the tones (frequency selectivity). That is, the more frequency-selective channel is, the smaller the averaging window should be. The relationship between the averaging window size and frequency selectivity (along with SNR) is studied in the next chapter.

Chapter 4

Estimator Performance and Simulation

4.1 Channel Models and Scenarios

There has been much effort in indoor channel modeling by many different groups, such as ETSI BRAN [23], ITU-R [31], and the IEEE 802.11 Working Group [46]. For example, the popular TGn channel models developed by the IEEE 802.11 for indoor WLAN are described in Table 4.1.

Although the channel models proposed by these institutes try to generalize the channel statistics for different environments, they lack details about the measurement settings, such as the shape or dimensions of the environment, physical orientation of obstacles, and the whereabouts of Tx/Rx. In addition, none of these models investigates the channel behaviour in other typical indoor environments, e.g., small/large office, corridor, or a large open space like foyer. To understand the channel behaviour in such environments, we

Parameter	Models					
	A	B	C	D	E	F
Avg 1st Wall Distance (m)	5	5	5	10	20	30
RMS Delay Spread (ns)	0	15	30	50	100	150
Maximum Delay Spread	0	80	200	390	730	1050
Number of Taps	1	9	14	18	18	18
Number of Clusters	1	2	2	3	4	6

Table 4.1: TGn Channel Model by the IEEE 802.11

have conducted several channel measurements at the University of Waterloo (UW). The measurement setups and environments are described in the following sections.

4.1.1 Measurement Setup

The channel measurement was performed using the Wireless open-Access Research Platform (WARP[1]) designed at the Rice University. The WARP platform, shown in Figure 4.1, is a programmable wireless research tool which provides a general environment for a clean-slate MAC/PHY development. There are three main components of the WARP platform that are of interest: (A) Xilinx Virtex-II Pro FPGA in which MAC protocols are written in C and targeted to embedded PowerPC cores, and PHY protocols are implemented within the FPGA fabric using MATLAB Simulink, (B) 2.4/5GHz Radio Board which supports wideband applications such as OFDM, and (C) 10/100 Ethernet port which serves as the interface between the board and the wired Internet.

The PHY/MAC implementation we adopted for the channel measurement is analogous to the mechanisms in the IEEE 802.11 which operates at channel 11 of 2.4GHz band with Carrier Sense Multiple Access with Collision Avoidance (CSMA/CA). The over-the-

[1]http://warp.rice.edu

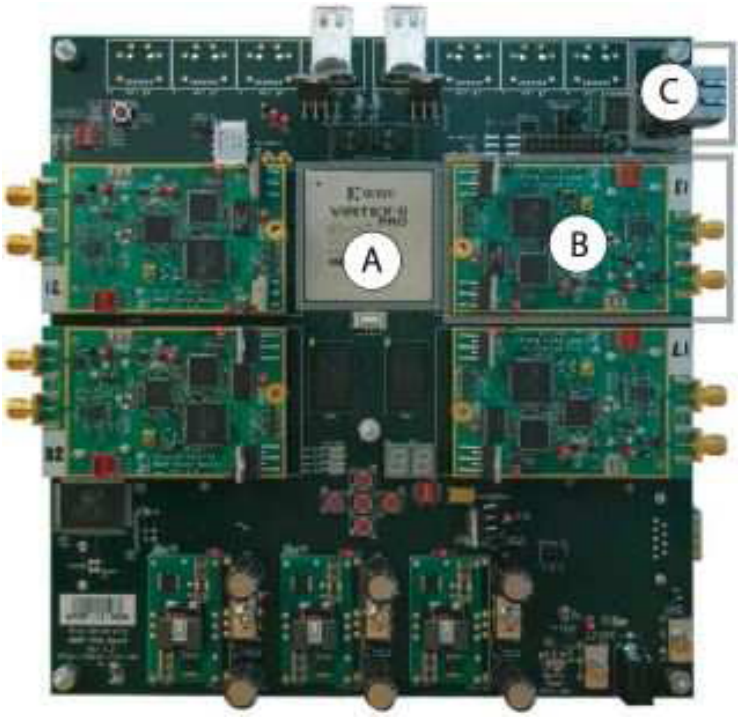

Figure 4.1: The WARP board as the IEEE 802.11 interface

air system bandwidth is 10MHz with a sampling rate of 40MHz. The OFDM symbol consists of 64 subcarriers (52 data subcarriers with 4 pilot subcarriers) and supports BPSK, QPSK, and 16-QAM modulation schemes. The PHY OFDM packet format is illustrated in Figure 4.2.

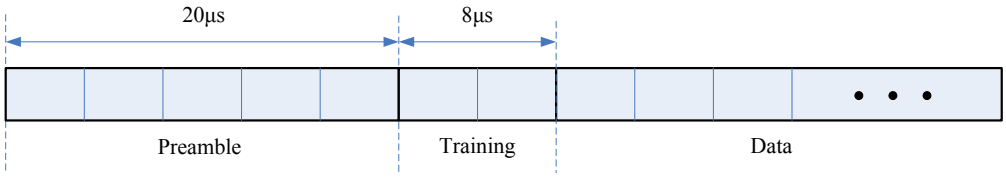

Figure 4.2: The OFDM packet structure for WARP implementation

The preamble is a hard-coded 320-sample (5 OFDM symbol length where one OFDM

symbol duration is 8 μs) sequence used by the receiver for AGC, carrier frequency offset estimation and symbol timing estimation. This field is analogous to that of Short Training Field (STF) in the IEEE 802.11a standard. The training field consists of a fixed sequence repeated one after another (2 OFDM symbol length) and it is mainly used for channel estimation, similar to Long Training Field (LTF) in the IEEE 802.11a. The channel estimation is performed such that the receiver independently estimates the channel using the LS method (refer to Section 3.1) for each training period and averages them out to produce a smoother channel estimate. This estimated channel is used for equalization and decoding in the data part until the next packet arrives.

Using this channel estimation method, the channel response in frequency domain was captured while we performed video streaming between two laptops each attached to a WARP board. The equipment setup is depicted in Figure 4.3.

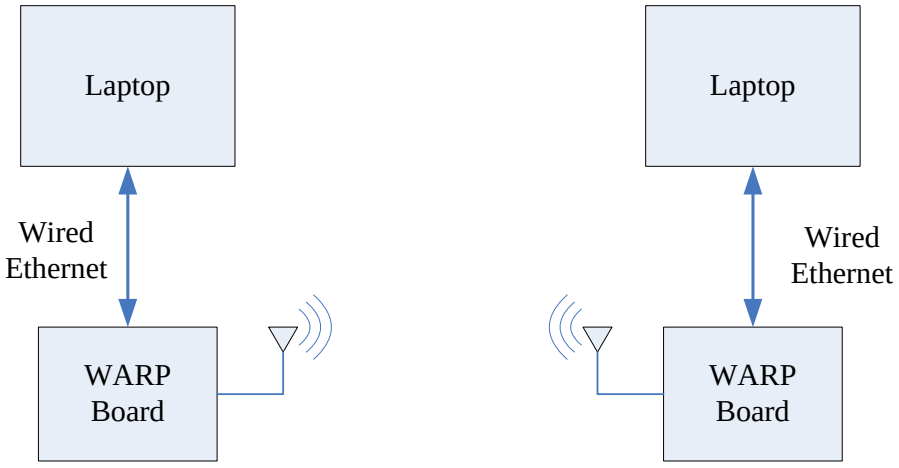

Figure 4.3: The equipment setup for channel measurement

4.1.2 Measurement Environments

The channel measurements were conducted on the second floor of South-East wing of Davis Centre (DC) building in the UW, where a fair mix of small offices, large offices, corridor, and wide open area are available. In this setup, we chose five different indoor environments which represent typical indoor scenarios where the WLAN is deployed. The description of the channel scenarios and their layouts in DC floor plan[2] are shown in Table 4.2 and Figure 4.4, respectively.

Scenario	**Condition**	**LOS distance (m)**	**Avg 1st wall distance (m)**	**Model**
Inside small office	LOS	3	3	A1
	NLOS	3	3	A2
Office - office	LOS	4	3	B1
	NLOS	4	3	B2
Corridor - corridor	LOS	8	2	C1
	NLOS	8	2	C2
Inside large office	LOS	8	5	D1
	NLOS	8	5	D2
WOA - WOA	LOS	15	10	E1
(wide open area)	NLOS	15	10	E2

Table 4.2: Description of channel scenarios

These locations were carefully chosen to represent the LOS and NLOS for each scenario. In case of channel model A2, C2 and E2, the effect of NLOS was artificially introduced by blocking the LOS with a large object, such as a desk or a cabinet.

The measurements were conducted during normal office hours with no restrictions imposed on the channel as people were free to move. Therefore the data collected and used

[2]Available at http://plantoperations.uwaterloo.ca/floor plans

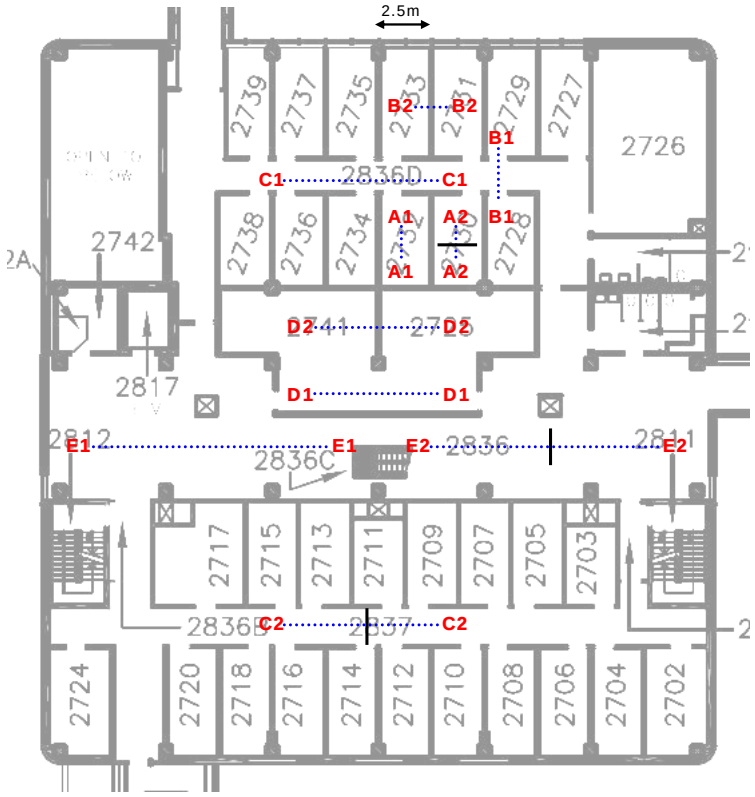

Figure 4.4: Layout of the channel scenarios at South-East wing of DC building

in the analysis are obtained from a realistic indoor radio environment and the statistical model deduced from this work is also practical for simulations explained in the next section. The channel capturing was conducted in such a way that both the Tx and Rx were fixed at one location as planned in Figure 4.4 and the snapshots of frequency channel estimate were recorded over time while the video images were transmitted over the air from one WARP board to another.

4.1.3 Measured Channel Frequency Responses

In Figure 4.5, we present the measured channel frequency responses using the WARP boards described previously. For each channel scenario, several responses were captured and their averaged response was calculated in order to eliminate the channel noise (shown as red and bold curve).

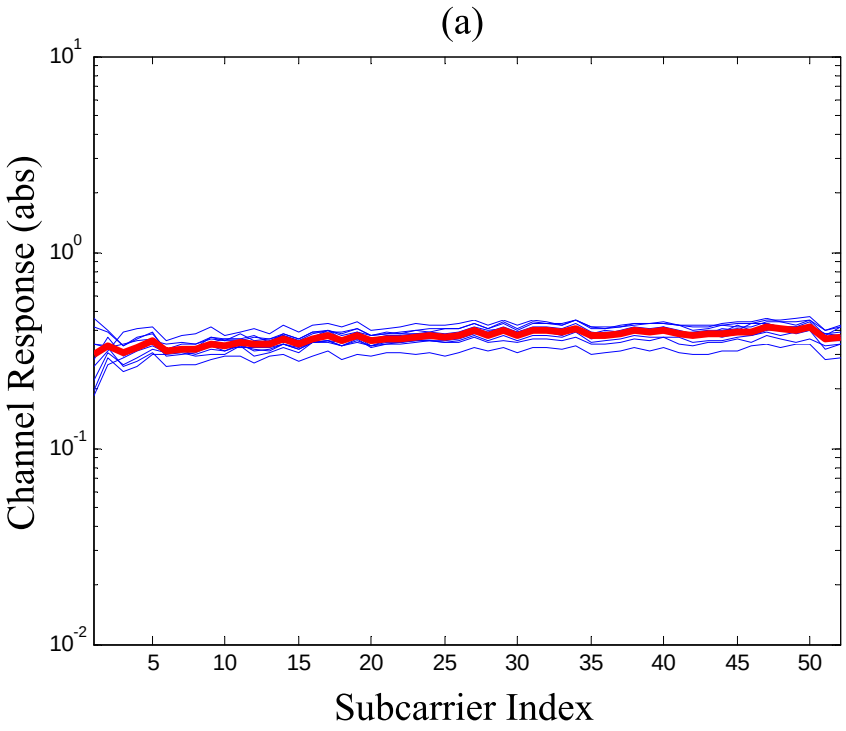

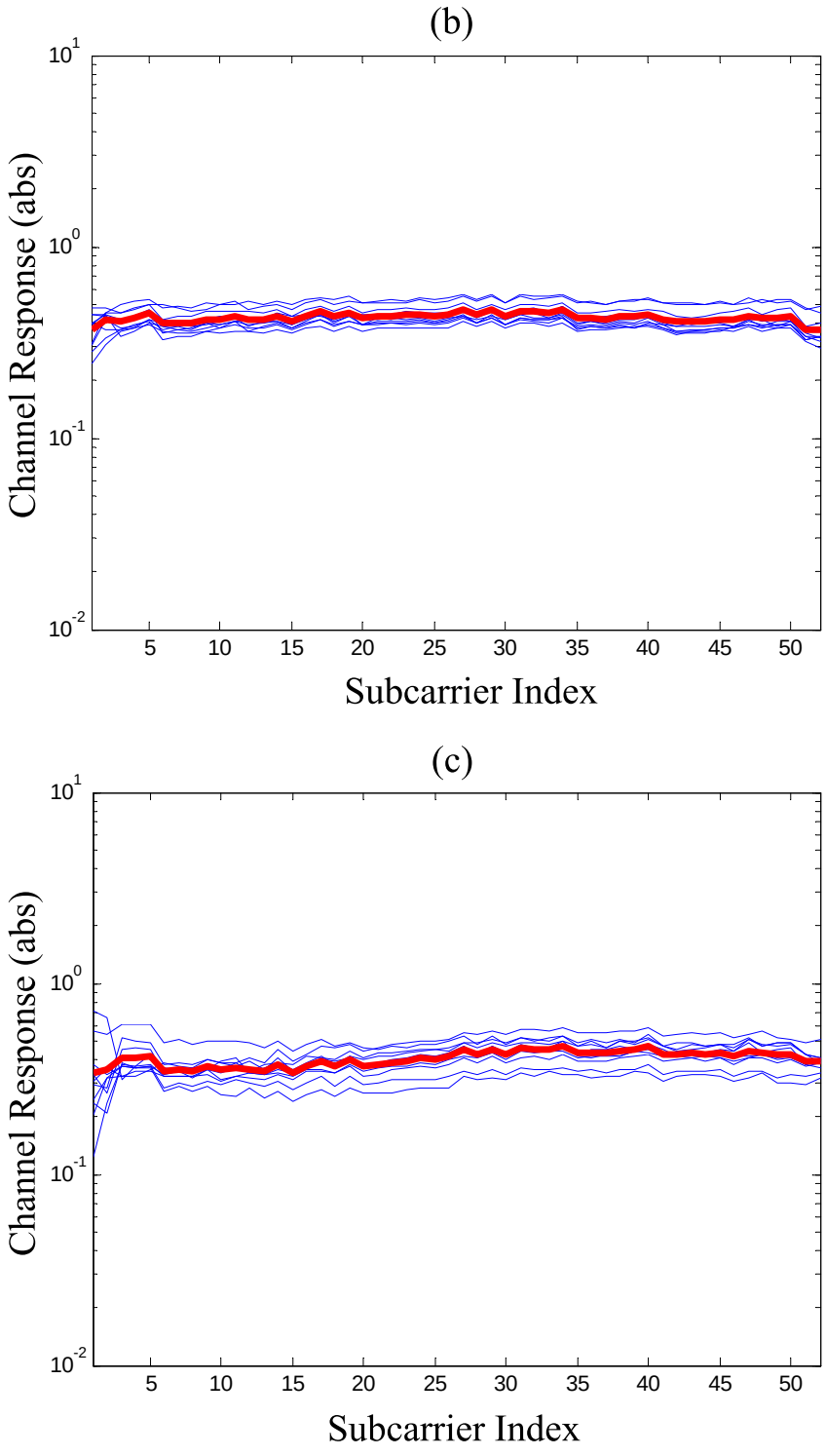
(b)
Channel Response (abs)
Subcarrier Index
(c)
Channel Response (abs)
Subcarrier Index

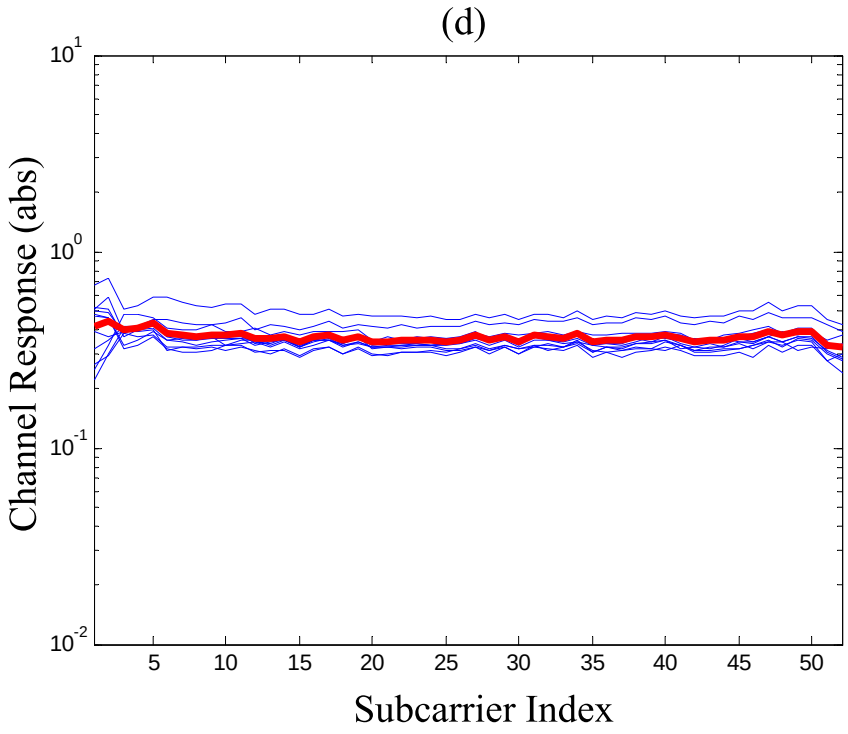
(d)
Channel Response (abs)
10^{1}
10^{0}
10^{-1}
10^{-2}
5
10
15
20
25
30
35
40
45
50
Subcarrier Index

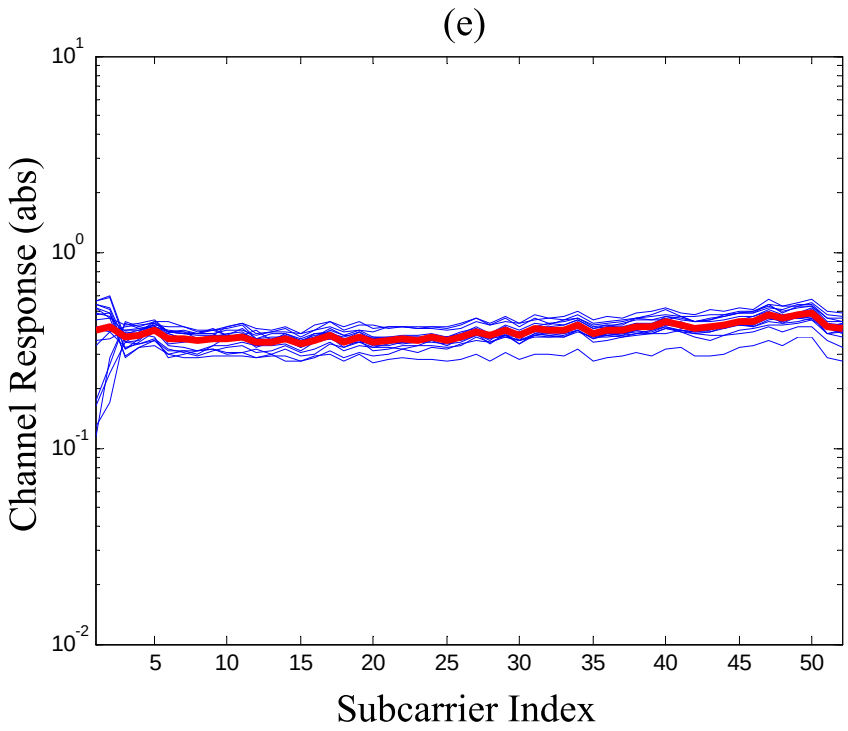
(e)
Channel Response (abs)
10^{1}
10^{0}
10^{-1}
10^{-2}
5
10
15
20
25
30
35
40
45
50
Subcarrier Index

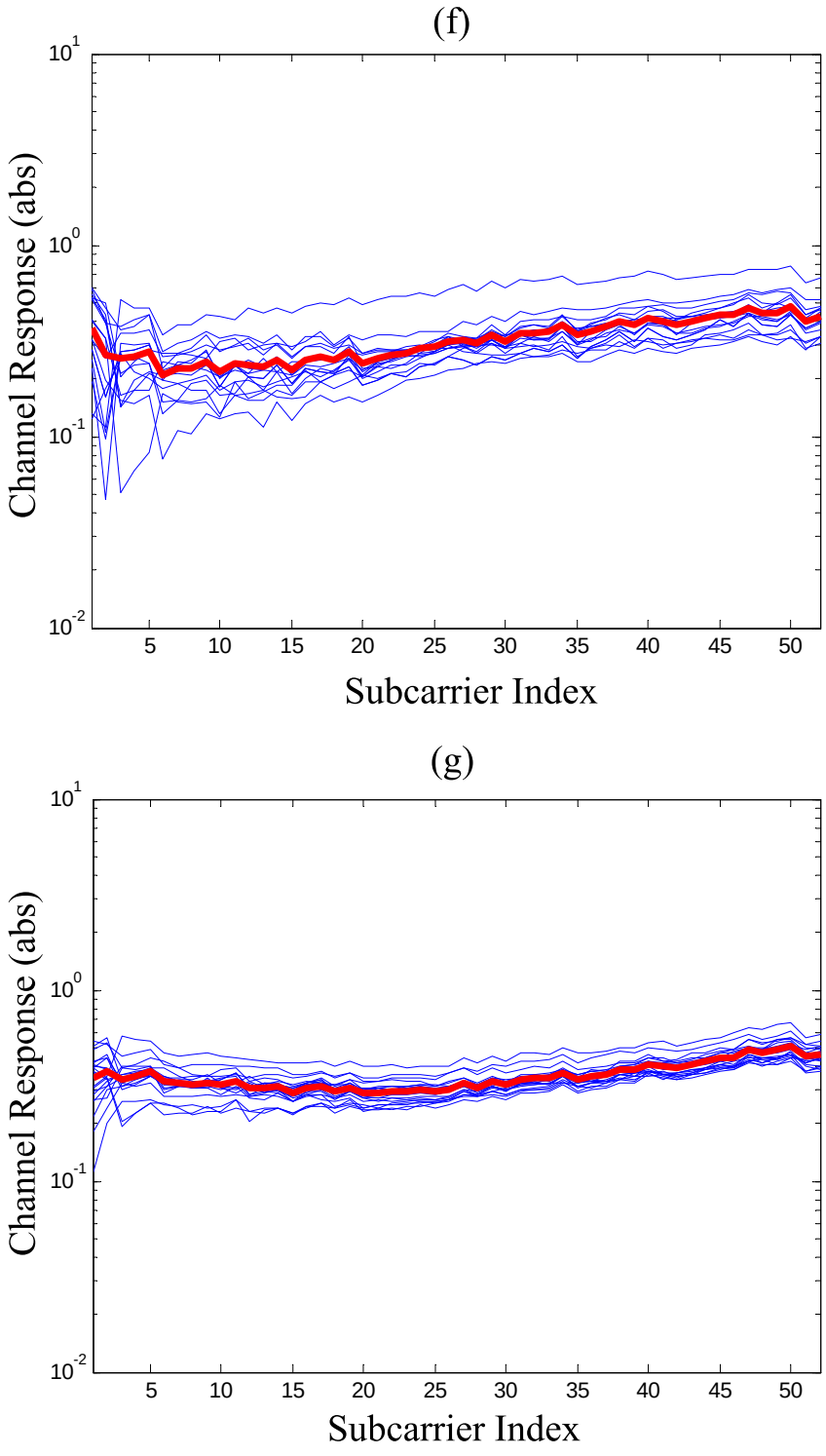
(f)
Channel Response (abs)
Subcarrier Index
(g)
Channel Response (abs)
Subcarrier Index

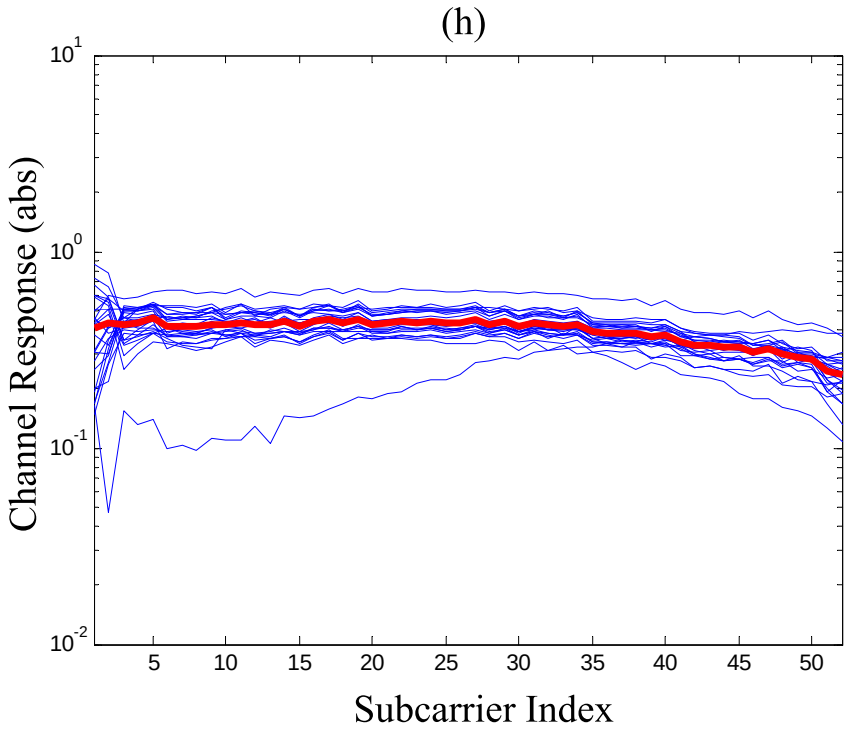
(h)
Channel Response (abs)
10^{1}
10^{0}
10^{-1}
10^{-2}
5
10
15
20
25
30
35
40
45
50
Subcarrier Index

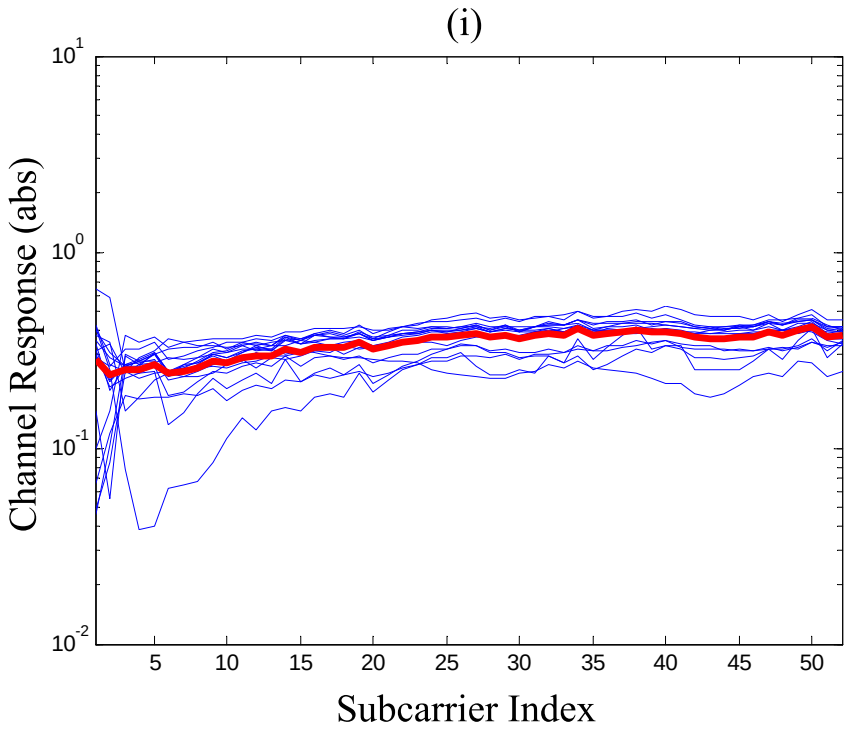
(i)
Channel Response (abs)
10^{1}
10^{0}
10^{-1}
10^{-2}
5
10
15
20
25
30
35
40
45
50
Subcarrier Index

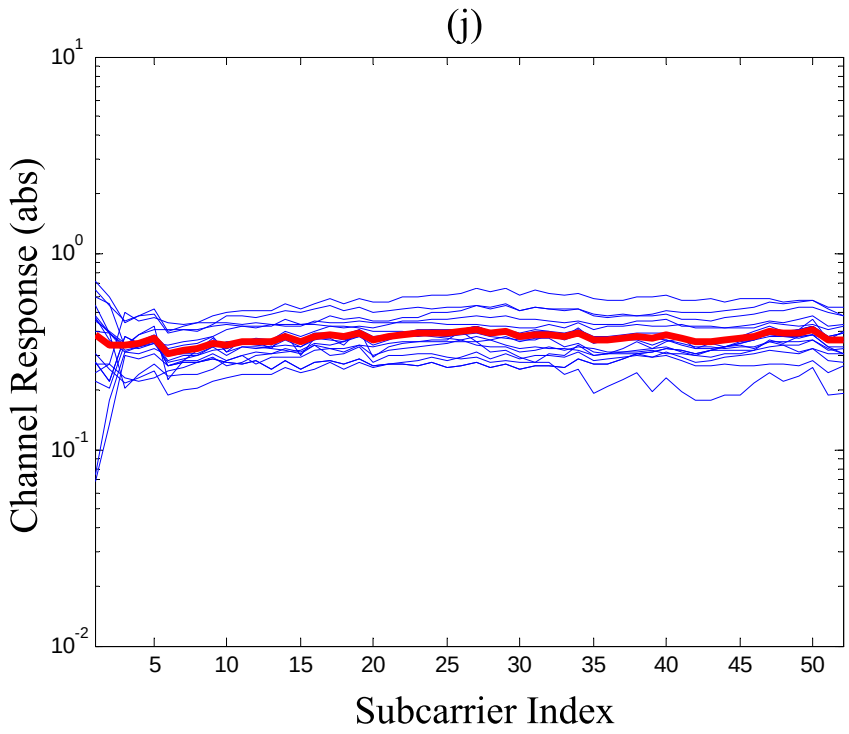

Figure 4.5: Channel frequency response for channel model (a) A1, (b) A2, (c) B1, (d) B2, (e) C1, (f) C2, (g) D1, (h) D2, (i) E1, and (j) E2

As shown in Figure 4.5, it is observed that the channel variations between consecutive packets increase as the dimensions of indoor environment are increased. In other words, the amount of variation from one channel response to another is increased over time. For example, most of the channel responses in scenario A1 are concentrated around the averaged response whereas many of responses deviating from the averaged response are observed in scenario E1. This is an interesting observation as the channel exhibits a *time selectivity* even though both Tx and Rx were set stationary for the entire time. Also, a theoretical coherence time is much larger than the time difference between capturing each consecutive responses. This can be explained by the fact that there are more traffic by people and changes in environment in a large office (D) or wide open area (E) than an area like a small office (A or B). To illustrate the finding more quantitatively, the variance per subcarrier of all the channel responses is calculated and then they are averaged out to represent the time variance for each channel scenario. In Figure 4.6, we see that the time variance increases proportionally with the size of the indoor environment, and this relationship is more evident in the NLOS cases. It is also observed that the variation is larger in case of LOS than of NLOS for a given channel scenario. We can then conclude that NLOS not only introduces frequency selectivity but also time selectivity in a wireless radio channel.

Another interesting finding is observed in the channel model C2. The radio propagation in a long and narrow indoor environment with very short distance to the surrounding walls exhibits a similar behaviour as in wide-open-area environment, when there is no dominant multipath component. This illustrates that the statistics of the channel are also significantly affected by the specific indoor settings and these factors should be taken into

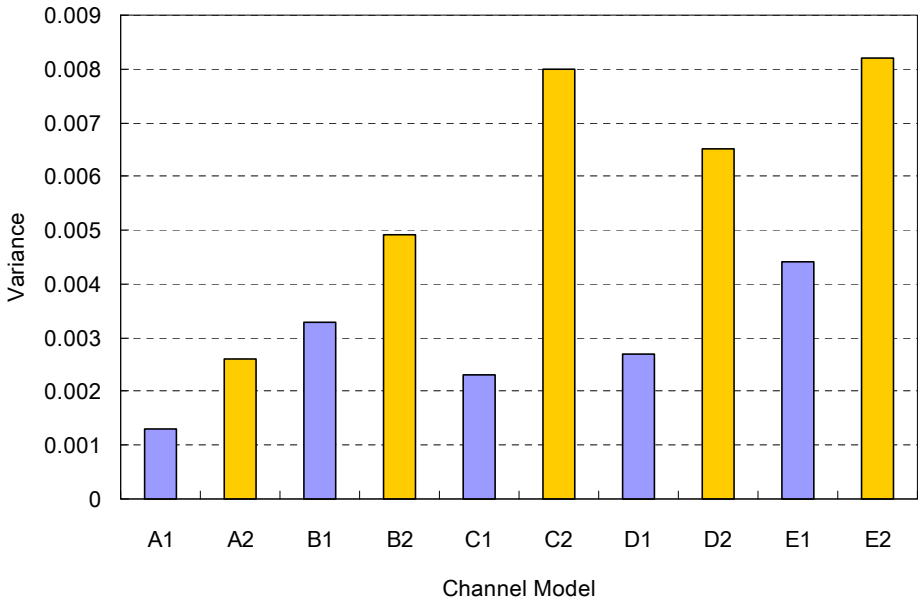

Figure 4.6: Variance of channel frequency response over time

account when designing an indoor wireless network such as WLAN.

In general, the channel response becomes more frequency selective as the distance between the Tx and Rx and/or the dimension of the indoor environment increases. However, the overall amount of channel fluctuation on average is insignificant (maximum 3dB in case of C2). Therefore, we conclude that the channel scenarios under investigation generally exhibit a frequency-flat.

4.2 Simulation Settings

The fundamental requirements and the parameters of the OFDM systems investigated for simulation are shown in Table 4.3. These parameters are chosen because they are the same as the ones that the WARP platform is used for its channel measurements. For simulation purposes, the characteristics of the above realistic channel models are translated into tapped-delayed-line models, where each channel model is represented with delays and their relative powers. The power intensity profile is listed in Table 4.4.

Parameter	**Specification**
Carrier frequency	$2.4GHz$
System Bandwidth	$10MHz$
Number of data subcarriers	52 (including 4 pilots)
FFT size	$N = 64$
CP length	16
Subcarrier frequency spacing	$\Delta f = 156.25kHz$ $(10MHz/64)$
OFDM symbol duration	$T_s = 8\mu s$ $(6.4\mu s + 1.6\mu s)$
Number of training symbols per packet	2
Number of data symbols per packet	20
Data symbol mapping	uncoded 16-QAM
Number of simulation runs per SNR	10000

Table 4.3: OFDM system parameters

In terms of modeling indoor channels using tapped delay line, we assume an exponentially decaying power-delay profile (linear in log-scale), but not necessarily uniformly distributed delays. We also assume that the only difference between LOS and NLOS is in the dominant LOS component and other multipath components are maintained the same. This means that the NLOS multipath components experience the same propagation behaviour as in the case of LOS setting.

Model	**Tap**	**Delay (ns)**	**Gain (dB)**
A1	1	0	0
	2	60	-19
A2	1	3	-0.9
	2	60	-19
B1	1	0	0
	2	120	-19.5
	3	200	-22.5
B2	1	3	-0.9
	2	120	-19.5
	3	200	-22.5
C1	1	0	0
	2	170	-17.2
	3	200	-22.5
C2	1	40	-6.5
	2	170	-17.2
	3	200	-22.5
D1	1	0	0
	2	210	-15.5
	3	290	-20.1
	4	340	-24.6
D2	1	4	-0.9
	2	210	-15.5
	3	290	-20.1
	4	340	-24.6
E1	1	0	-4.5
	2	230	-20.7
	3	380	-23.5
	4	420	-26.6
E2	1	150	-5.3
	2	230	-20.7
	3	380	-23.5
	4	420	-26.6

Table 4.4: Indoor channel models using tapped delay line

4.3 MSE Performance

From Figure 4.7 to Figure 4.16, we compare the normalized MSE of the proposed channel estimators: MMSE-exponential-Rhh and AW, for the channel models described in Section 4.1. The normalized MSE of the LS and MMSE by Edfors [34] (simply MMSE henceforth for readability) are also included for performance comparison. Here, the normalized MSE is defined as

$$MSE_{normalized} = E\left\{(\hat{\boldsymbol{h}} - \boldsymbol{h})^H(\hat{\boldsymbol{h}} - \boldsymbol{h})/\boldsymbol{h}^H\boldsymbol{h}\right\} \tag{4.1}$$

, where $\hat{\mathbf{h}}$ and $\mathbf{h}$ are the estimated and true channel response, respectively.

First, we observe that the proposed modified MMSE estimator, MMSE-exponential-Rhh, performs better than the LS estimator at low SNR and performs almost the same as the LS estimator at high SNR. The MMSE-exponential-Rhh estimator also outperforms the MMSE estimator in NLOS channel scenarios where the irreducible MSE floors by MMSE estimator are much more severe than that of the proposed estimator. For example, in Figure 4.12, the performance degradation of the MMSE estimator is more apparent than other proposed estimator. This irreducible error floor is due to the channel parameter mismatch by the MMSE estimator. Namely, the MMSE estimator's channel correlation matrix $\boldsymbol{R_{hh}}$ is modeled using TGn channel model in Table 4.1, while the actual channel is modeled using the parameters in Table 4.4. The assumption of uniformly distributed delays over the length of the CP also contributes to the channel mismatch when the true channel is clearly not the case. Although the MMSE estimator may perform the best under the perfect channel match, we find that it is not practical and cannot guarantee the best

performance under many indoor environments. On the other hand, our proposed estimator is rather *loosely* based on the true channel statistics and shown to be much more robust against the channel mismatch.

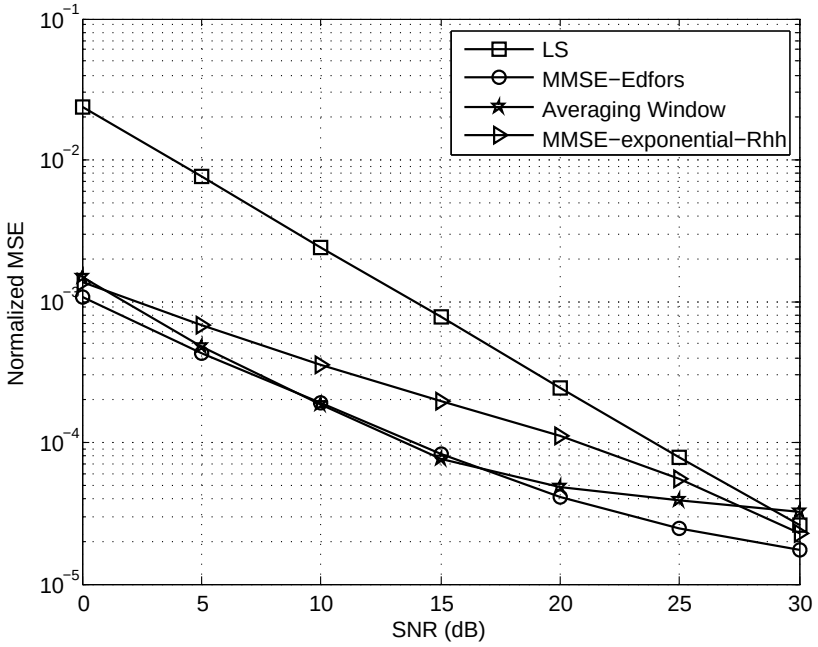

Figure 4.7: Normalized MSE for channel model A1

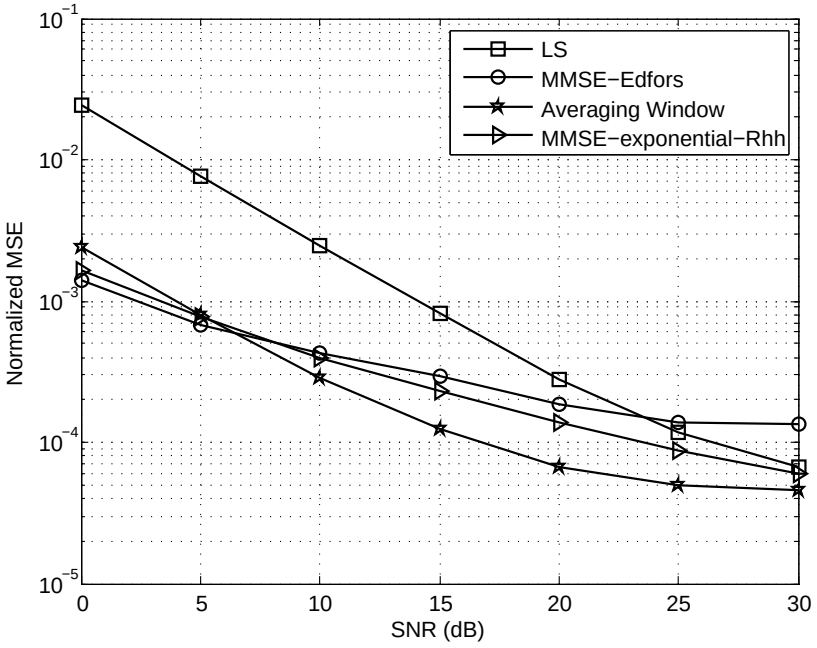

Figure 4.8: Normalized MSE for channel model A2

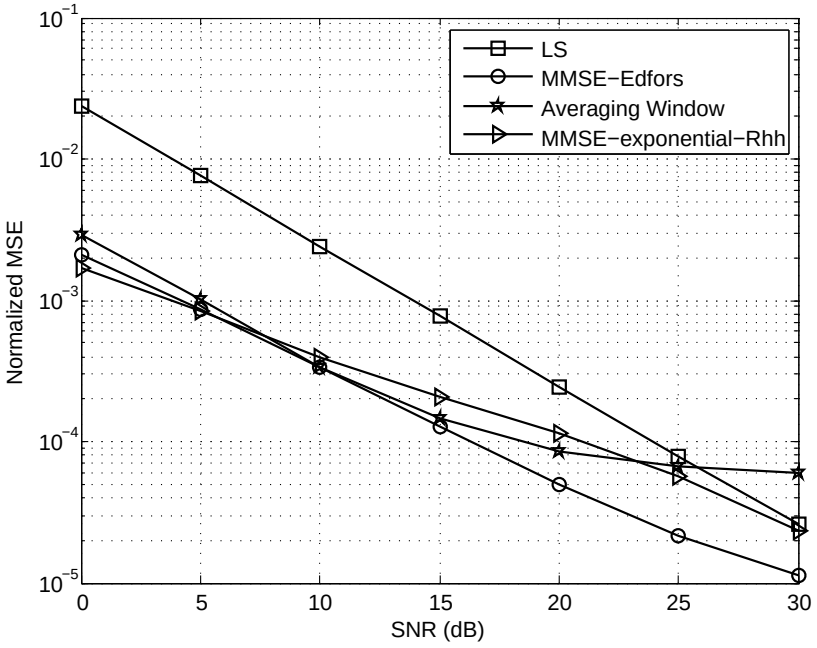

Figure 4.9: Normalized MSE for channel model B1

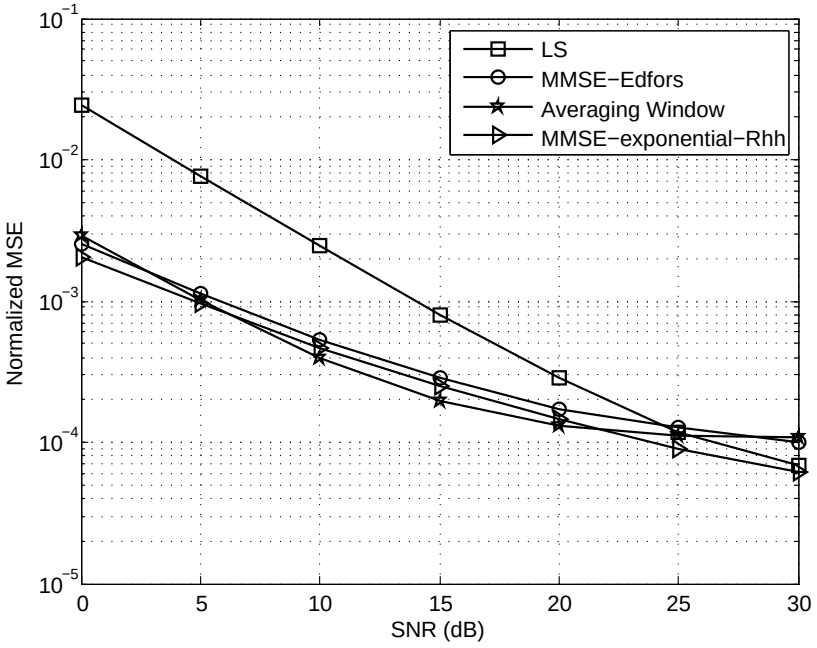

Figure 4.10: Normalized MSE for channel model B2

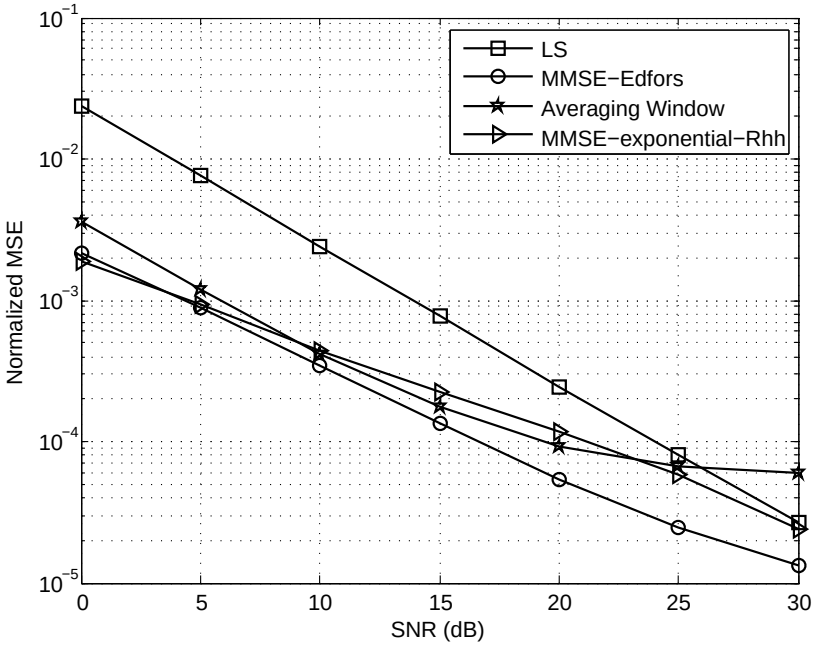

Figure 4.11: Normalized MSE for channel model C1

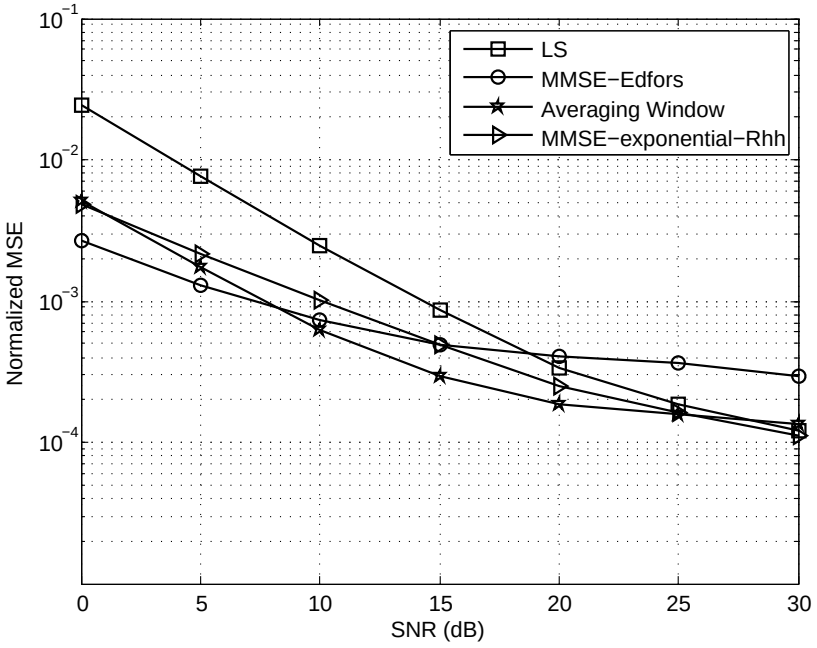

Figure 4.12: Normalized MSE for channel model C2

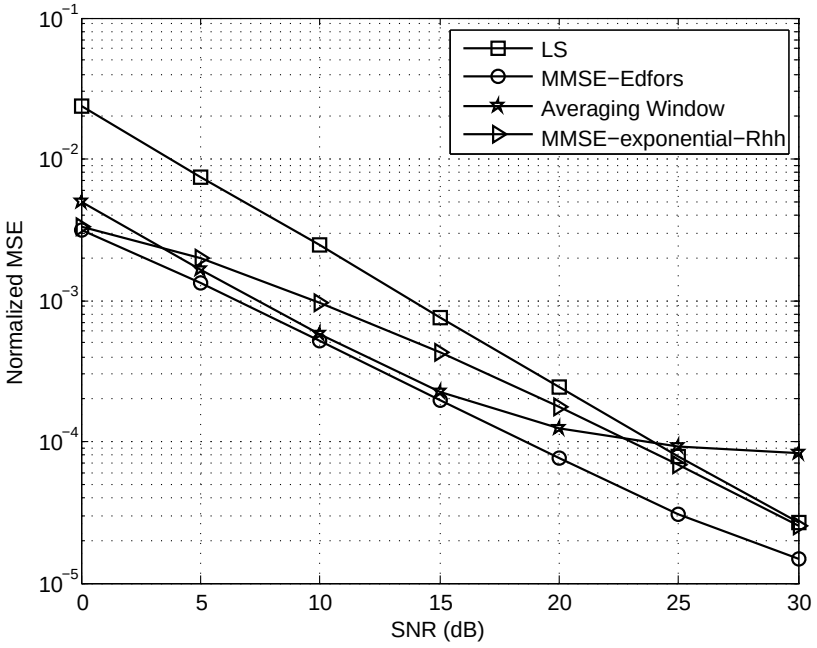

Figure 4.13: Normalized MSE for channel model D1

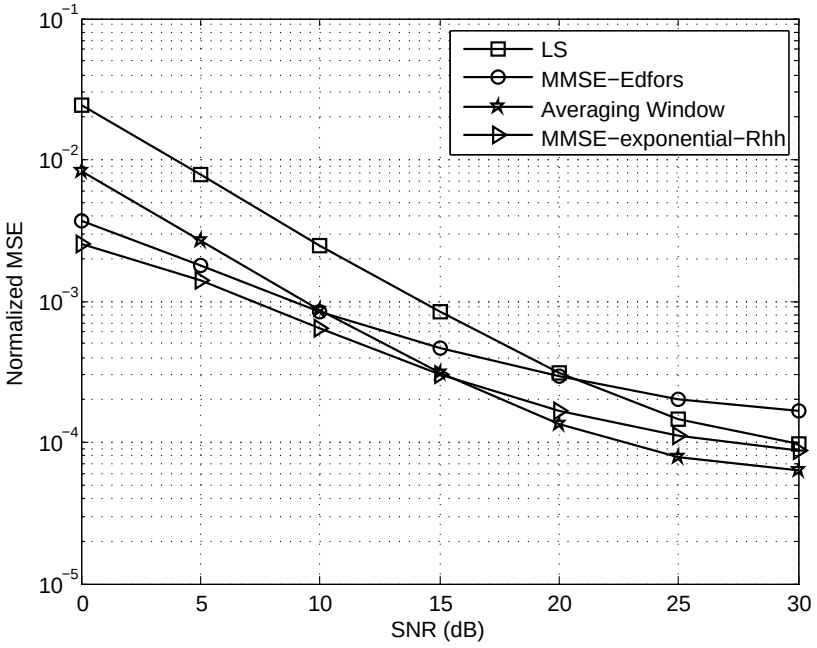

Figure 4.14: Normalized MSE for channel model D2

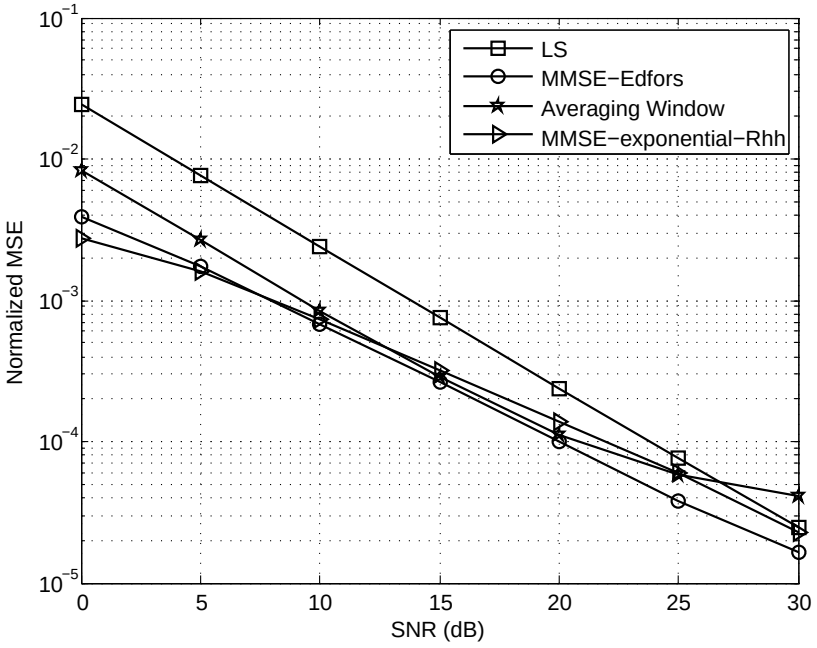

Figure 4.15: Normalized MSE for channel model E1

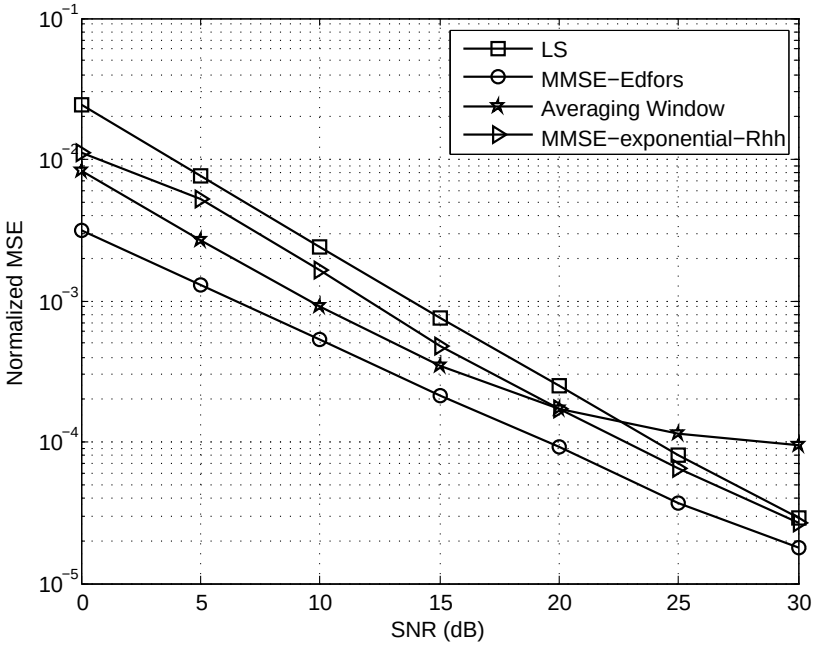

Figure 4.16: Normalized MSE for channel model E2

Secondly, the AW estimator shows that it is very effective in reducing noise at middle SNR range (10 to 20dB). The averaging window size is chosen such that it minimizes the MSE across all SNR regions since there is a trade off between the size of averaging window and performance gain. For example, a large averaging window size is preferable at low SNR in order to minimize the effect of noise. On the other hand, a small averaging window size is more desirable at high SNR otherwise the performance will become worse than that of the LS estimator. This trade off is illustrated in Figure 4.17, where the averaging window size is naturally optimized for middle SNR range.

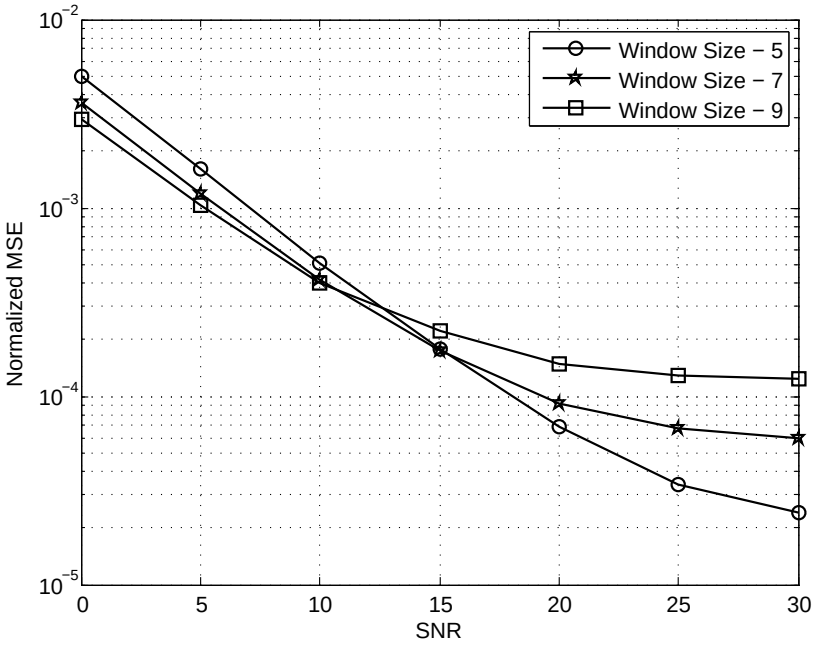

Figure 4.17: Effects of averaging window size for channel model C1

4.3.1 Significance of ρ in MMSE-Exponential-Rhh Method

In this section, we analyze the relationship between the correlation parameter ρ (in MMSE-exponential-Rhh estimator) and the channel models. In Figure 4.18, the ρ value calculated by equation (3.14) for each channel model is plotted.

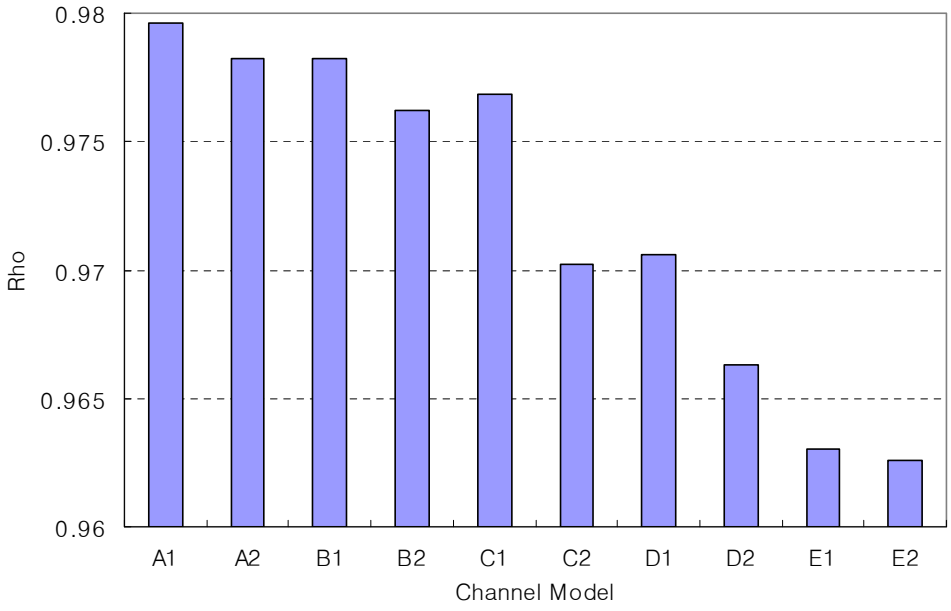

Figure 4.18: Correlation parameter ρ for each channel model

As expected, the correlation parameter decreases as the channel experiences more frequency selectivity. A legitimate question at this point is: how well does the correlation parameter ρ in MMSE-exponential-Rhh estimator reflect the channel statistics in terms of minimizing the MSE? How sensitive is the MSE performance towards the parameter mismatch? In Figure 4.19, we plot the MSE performance of the MSE-exponential-Rhh estimator when several values of ρ are used in the channel scenario A1, in order to illustrate the effect of parameter mismatch. The actual ρ value for this channel is calculated to be

0.9796.

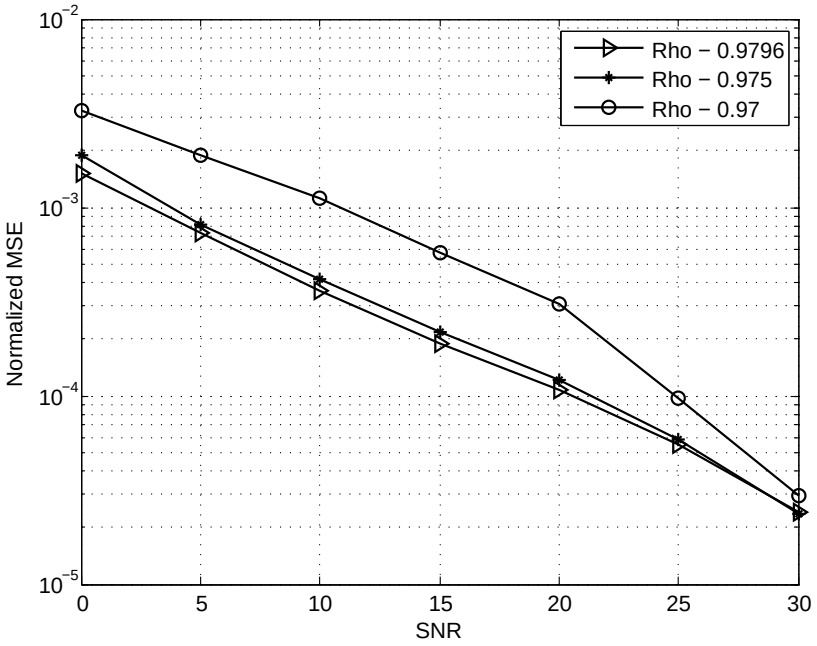

Figure 4.19: Influence of ρ in MMSE-exponential-Rhh estimator for channel model A1

From the results in Figure 4.19, we observe that the MSE curves are very sensitive to changes in ρ and even a minor mismatch can cause a significant performance degradation. Thus the MMSE-exponential-Rhh estimator requires a precise correlation calculation for the best performance.

4.3.2 Significance of the Averaging Window Size in AW Method

We investigate the relationship between the averaging window size in AW method and the frequency selectivity for each channel model. The frequency selectivity for each channel scenario is quantified by calculating a variance of the channel frequency response across the tones. The optimal averaging window size and the variance of the channel frequency

response are compared in Figure 4.20.

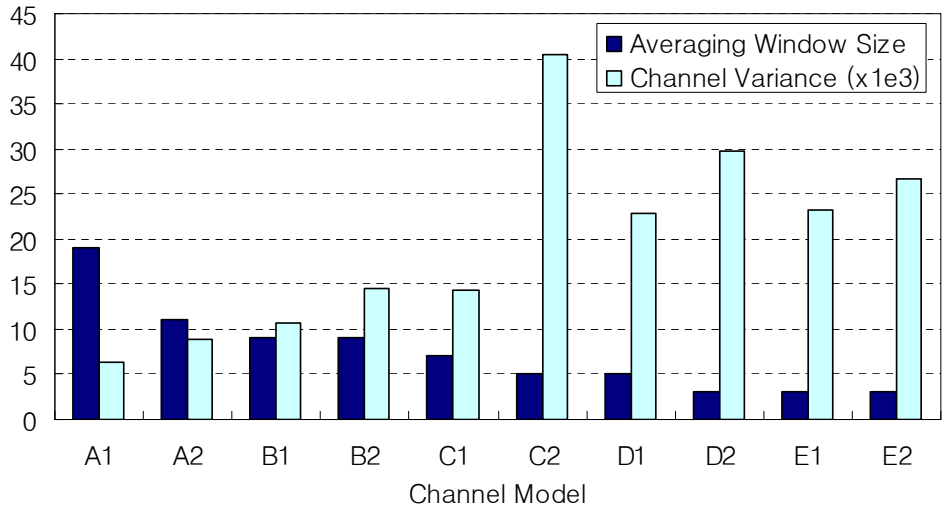

Figure 4.20: Relationship between the averaging window size and the frequency selectivity

It is shown that the size of averaging window gets smaller as the channel variance across the tones increases. We see that the window size reaches its minimum value[3] once the channel variance exceeds 0.02. This means that the AW estimator will always have a minimum averaging window size for any channel worse than the channel scenario D2 and its performance will be limited. Therefore it is recommended that the AW method should be used under the frequency-flat channel for a maximum design flexibility.

4.4 BER Performance

We study the BER performance of the proposed channel estimators under realistic indoor channel environments described in Section 4.1.2. In Figure 4.21 and Figure 4.22, we present

[3]The minimum averaging window size is set to 3 since the size is set to be odd number and the size of 1 has no effect.

the BER results for the proposed methods along with the LS and MMSE estimators for channel model A1 and C2. The results with perfect channel knowledge are also given for comparison. For complete BER performance results in all channel models, see Appendix A.

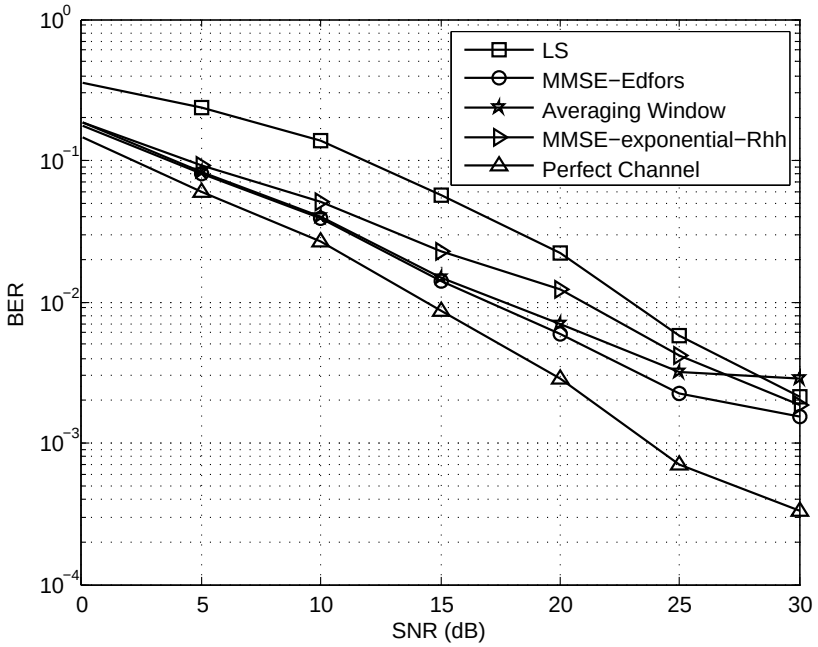

Figure 4.21: BER performance for channel model A1

As predicted from the MSE performance analysis, the proposed estimators outperform the LS estimator under all channel scenarios, except the AW estimator at high SNR. We observe that the MMSE-exponential-Rhh estimator typically has 2-3dB performance gain over the LS estimator when BER is 10^{-2}. For the same BER, the AW estimator also shows a superior performance gain over the LS estimator especially when the channel is very flat across the tones. For example, in Figure 4.21, the AW estimator has about 5dB gain compared to that of the LS estimator. Furthermore, it has almost the same performance

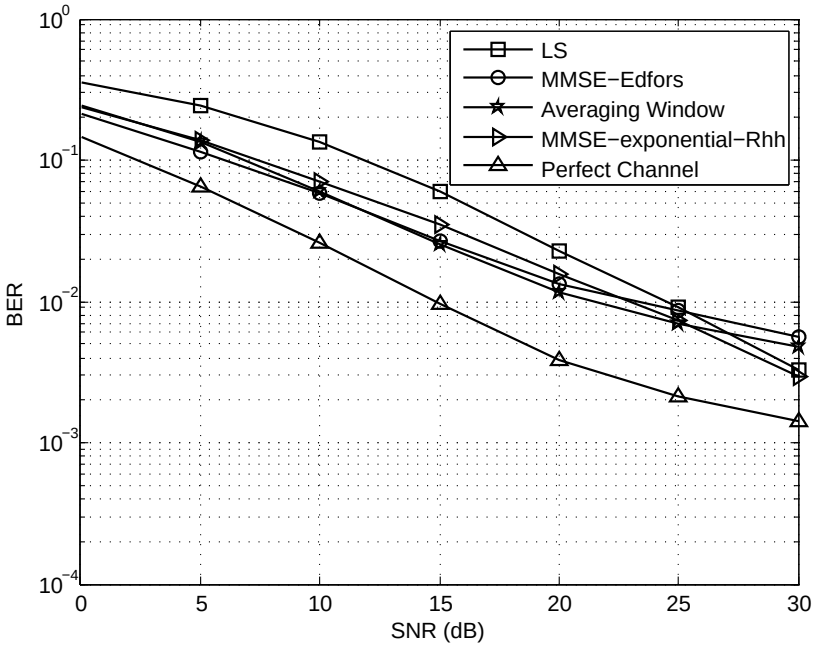

Figure 4.22: BER performance for channel model C2

as the MMSE estimator at low and mid SNR range.

From Figure 4.22 in which the channel exhibits a lot of time variations, the MMSE and AW estimators show a trend of BER floor at high SNR whereas the MMSE-exponential-Rhh estimator continuously brings the BER curves below the LS estimator. In fact, their BER performance at low-to-mid SNR range is very comparable to that of the MMSE estimator. This shows that the performance loss by modeling the channel correlation matrix *Rhh* with an exponential and/or linear function is insignificant, and they are also robust against the changes of the channel in time.

In comparison between the proposed methods, the MMSE-exponential-Rhh estimator shows a similar BER performance as the AW estimator at low and mid SNR range, but better in suppressing the BER at high SNR range.

Chapter 5

Conclusion and Future Work

With ever-increasing interest in OFDM and its adoption in many wireless communication systems such as the IEEE 802.11, channel estimation becomes one of the most essential tasks in compensating distortion from the channel. Although active investigation in this area has resulted in a variety of research, there has been very little effort in understanding typical indoor environments and designing channel estimation schemes that are both robust and practical for such channel conditions.

In this work, we have proposed two simple channel estimation techniques: MMSE-exponential-Rhh that is based on the traditional MMSE estimator with the channel correlation matrix modeled by exponential function, and AW estimator which is based on the *sliding window* averaging the LS estimate across the frequency tones. We have also measured the channel frequency responses under 10 different typical indoor channel scenarios and translated their information into tapped-delayed-line models for simulation purposes.

The channel measurements have shown that the statistics of the channel are affected not only by the distance between Tx and Rx, but also by the physical orientation of the

particular indoor environment. Although the channel statistics differ from one to another, it is shown that the variances of their channel frequency responses are insignificant and the channels under investigation can be considered as frequency-flat.

The simulation results have demonstrated that all of our proposed estimators outperform the LS estimator under all channel models. In general, the MMSE-exponential-Rhh estimator gives about 2-3 dB improvement over the LS estimator while maintaining robustness under channel mismatch. The investigation also shows that AW estimator performs the best especially at low and mid SNR range, offering up to 5 dB performance gain. It is recommended that the AW estimator would be used in low-to-mid SNR range and the MMSE-exponential-Rhh estimator at high SNR range.

For future research, developing a hardware implementation of our proposed schemes on WARP boards and conducting their BER performance under the same channel scenarios are of great interest. To build upon this thesis, the performance evaluation of the proposed schemes under more severe time- and frequency-selective channel can also be considered. Another interesting future research would be an investigation into further improving the AW estimator by adaptively adjusting its window size depending on the system SNR, and/or multiplying the LS estimates by the optimal weights before averaging as to minimize the MSE.

Appendix A

BER Performance for All Channel Models

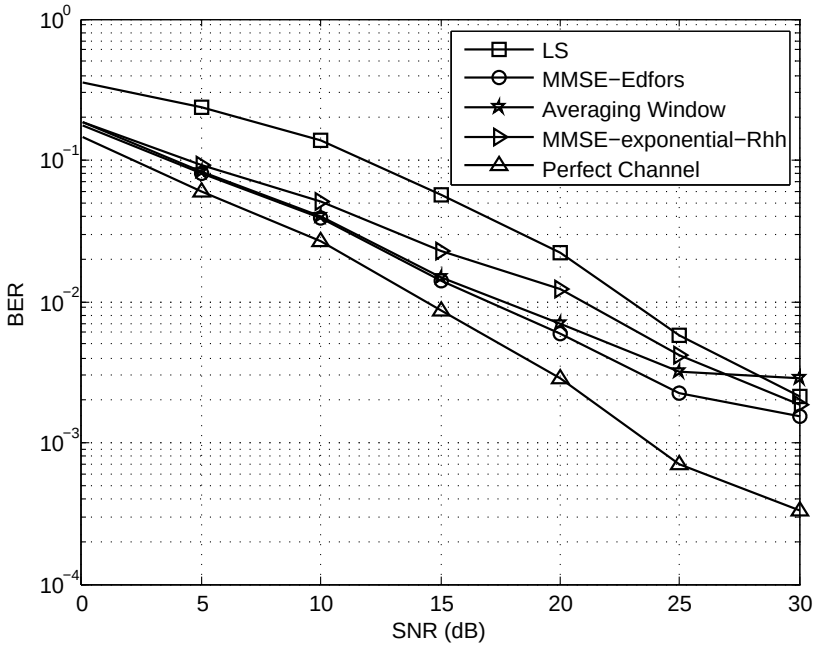

Figure A.1: BER performance for channel model A1

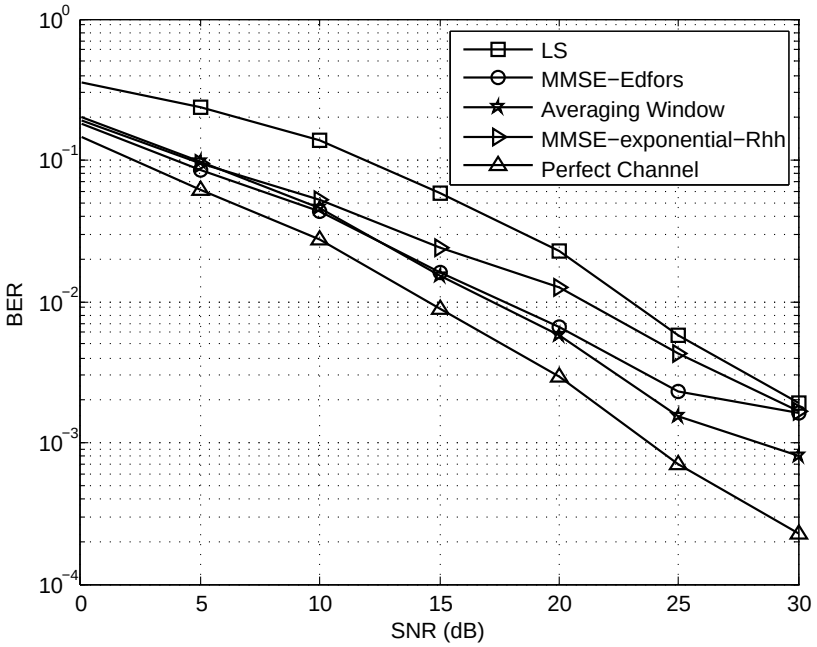

Figure A.2: BER performance for channel model A2

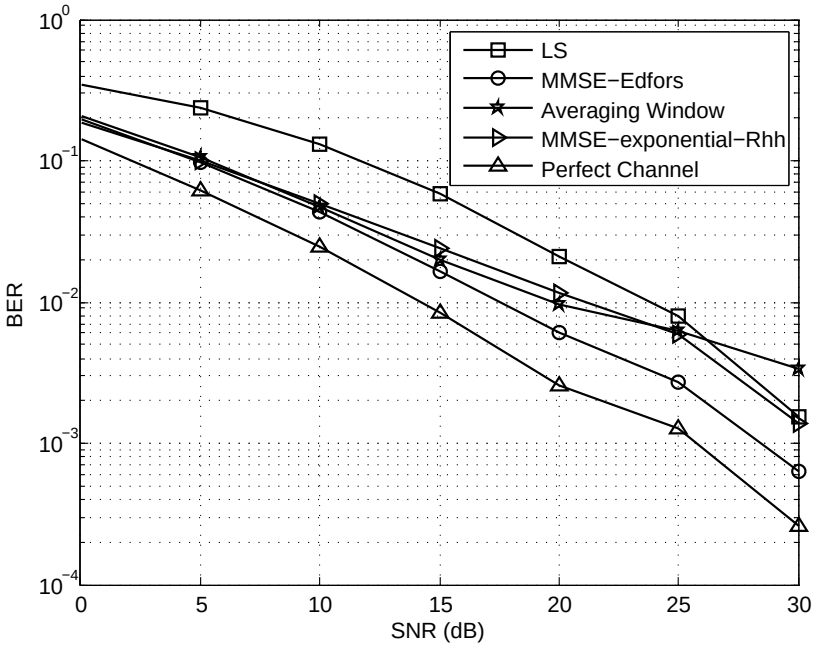

Figure A.3: BER performance for channel model B1

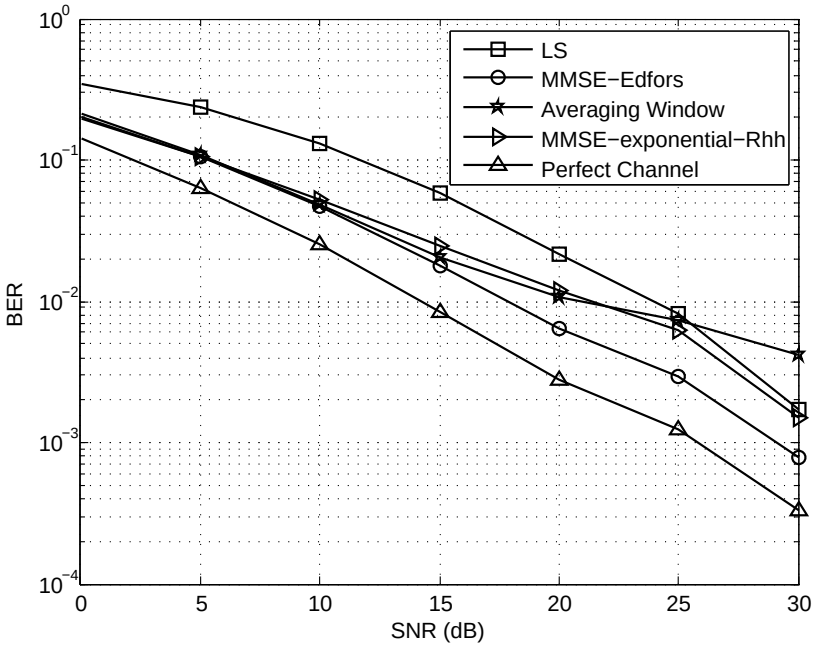

Figure A.4: BER performance for channel model B2

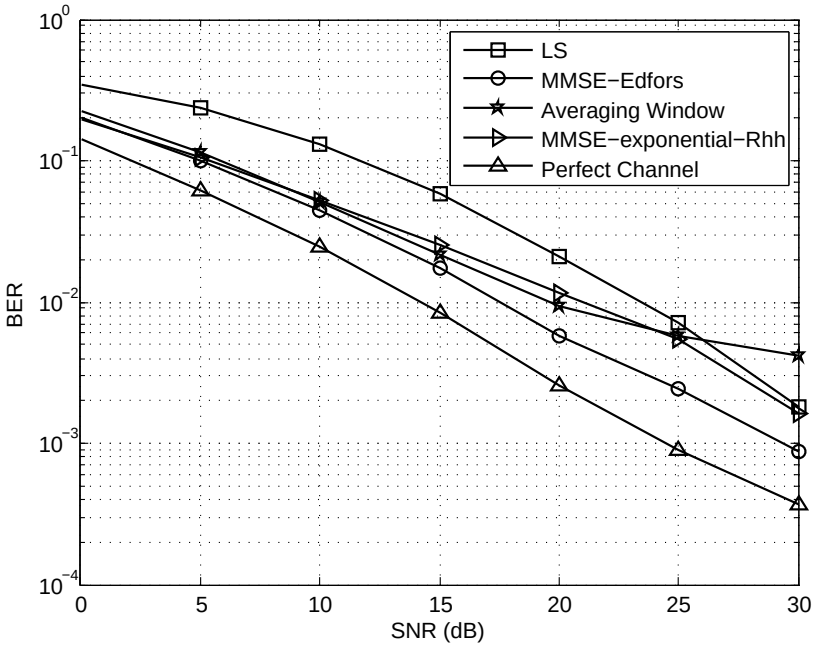

Figure A.5: BER performance for channel model C1

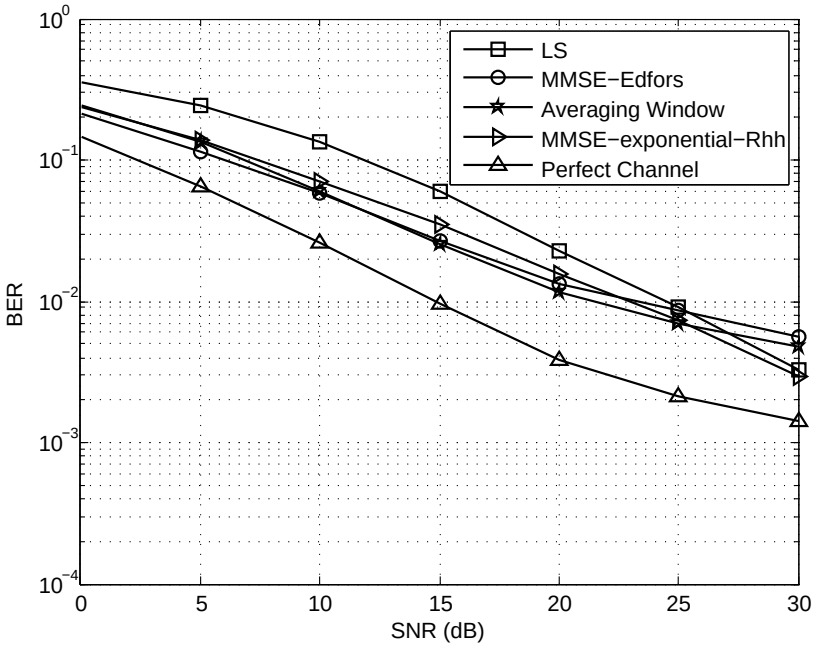

Figure A.6: BER performance for channel model C2

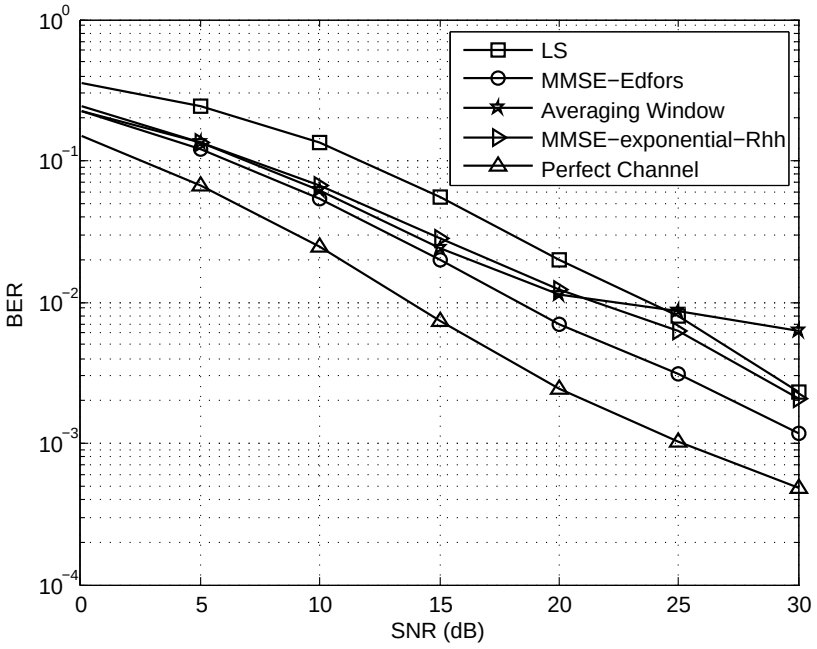

Figure A.7: BER performance for channel model D1

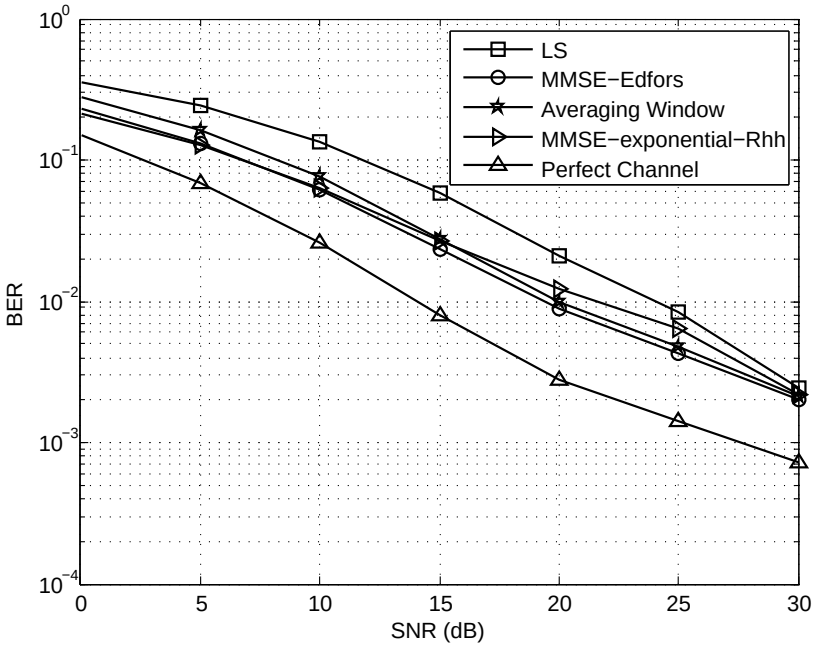

Figure A.8: BER performance for channel model D2

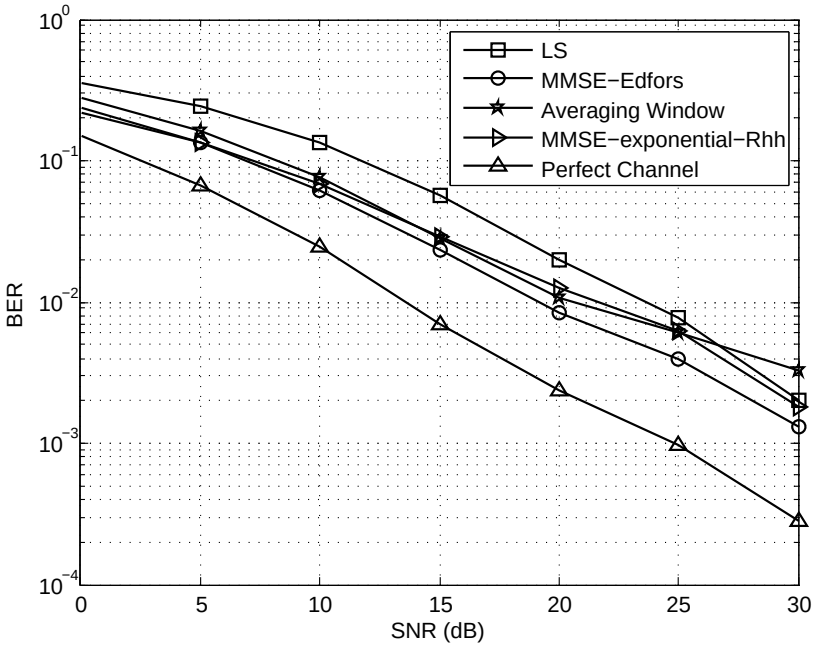

Figure A.9: BER performance for channel model E1

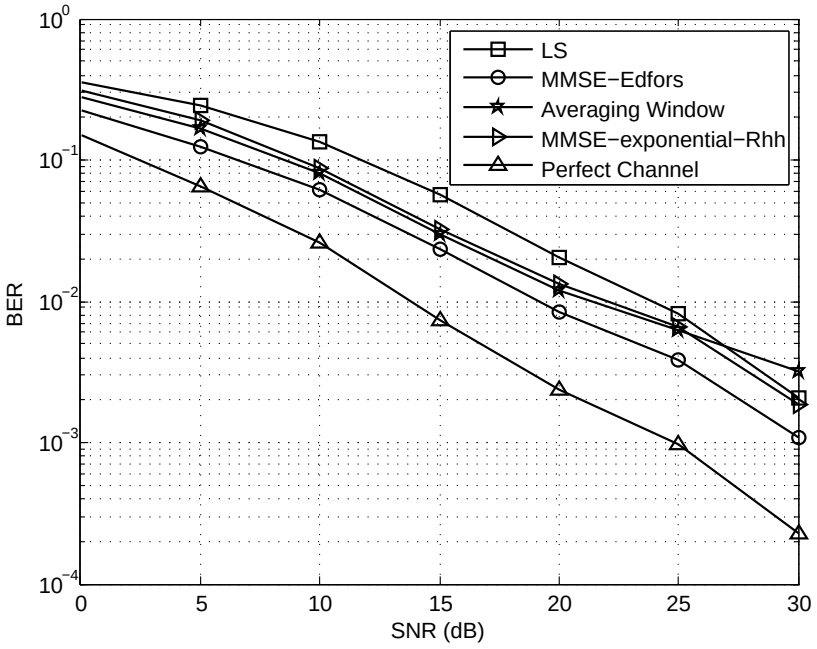

Figure A.10: BER performance for channel model E2

References

[1] IEEE Standard 802.11a 1999. *Wireless LAN Medium Access Control (MAC) and Physical Layer (PHY) Specifications: High-speed Physical Layer in the 5GHz Band.* IEEE, September 1999.

[2] IEEE Standard 802.11b 1999. *Wireless LAN Medium Access Control (MAC) and Physical Layer (PHY) Specifications: High-speed Physical Layer in the 2.4GHz Band.* IEEE, September 1999.

[3] IEEE Standard 802.11g 2003. *Wireless LAN Medium Access Control (MAC) and Physical Layer (PHY) Specifications: Future Higher Data Rate Extension in the 2.4 GHz Band.* IEEE, September 2003.

[4] IEEE Standard 802.11nD2.00 2007. *Wireless LAN Medium Access Control (MAC) and Physical Layer (PHY) Specifications: Enhancements for Higher Throughput.* IEEE, September 2007.

[5] IEEE Standard 802.16e 2005. *Local and Metropolitan Area Networks - Part 16, Air Interface for Fixed Broadband Wireless Access Systems.* IEEE, September 2005.

[6] R. Zhang A. P. Petropulu and R. Lin. Blind ofdm channel estimation through simple linear precoding. *IEEE Trans. Wireless Commun.*, 3(2):647–655, Mar. 2004.

[7] C. R. N. Athaudage and A. D. S. Jayalath. Enhanced mmse channel estimation using timing error statistics for wireless ofdm systems. *IEEE Trans. Broadcast.*, 50(4), Dec. 2004.

[8] X. You J. Wang B. Han, X. Gao and E. Costa. An iterative joint channel estimation and symbol detection algorithm applied in OFDM system with high data to pilot power ratio. In *Proc. IEEE Int'l. Conf. Commun.*, volume 3, pages 2076–2080, Anchorage, AK, May 2003.

[9] L. Hanzo B. J. Choi, T. Keller and M. Munster. *OFDM and MC-CDMA for Broadband Multi-User Communications, WLANs and Broadcasting.* Wiley-IEEE Press, Aug. 2003.

[10] N. C. Beaulieu C. C. Tan. On first-order markov modeling for the rayleigh fading channel. *IEEE Trans. Commun.*, 48(12), Dec. 2000.

[11] X. Cai and A. N. Akansu. A subspace method for blind channel identification in OFDM systems. In *Proc. ICC*, pages 929–933, New Orleans, LA, Jul. 2000.

[12] J. Cho. A novel channel estimation method for ofdm in high-speed mobile system. In *Proc. IEEE Int'l. Symp.Ind. Electron.*, volume 1, pages 571–74, Pusan, Korea, Jun. 2001.

[13] R. H. Clarke. A statistical theory of mobile-radio reception. In *Bell Syst. Tech. J.*, volume 47, pages 957–1000, 1968.

[14] G. Matz D. Schafhuber and F. Hlawatsch. Adaptive wiener filters for time-varying channel estimation in wireless OFDM systems. In *Proc. IEEE Int'l Conf. Acoust., Speech, and Signal Processing*, volume 4, pages 688–91, Hong Kong, China, Apr. 2003.

[15] J. Cardoso E. Moulines, P. Duhamel and S. Mayrargue. Subspace methods for the blind identification of multichannel fir filters. *IEEE Trans. Signal Process.*, 43(2):516–525, Feb. 1995.

[16] M. Engels. *Wireless OFDM Systems: How to Make Them Work?* Kluwer Academic Publishers, 2002.

[17] S. W. McLanughln Y. Li M. A. Ingram G. L. Stuber, J. R. Barry and T. G. Pratt. Broadband mimo-ofdm wireless communications. *Proceedings of the IEEE*, 92(2), Feb. 2004.

[18] F. Gao and A. Nallanathan. Blind channel estimation for ofdm systems via a generalized precoding. *IEEE Trans. Vehicular Technol.*, 56(3):1155–1164, May 2007.

[19] R. W. Heath and G. B. Giannakis. Exploiting input cyclostationarity for blind channel identification in ofdm systems. *IEEE Trans. Signal Process.*, 47:848–856, Mar 1999.

[20] M. Hsieh and C. Wei. Channel estimation for ofdm systems based on comb-type pilot arrangement in frequency selective fading channels. *IEEE Trans. Consumer Electron.*, 44(1), Feb. 1998.

[21] Eur. Telecommun. Stand. Inst. *Broadband Radio Access Networks (BRAN): High*

Performance Radio Local Area Networks (HYPERLAN), Type 2; Systems Overview. ETR 101 683 114, 1999.

[22] M. Sandell S. K. Wilson J. J. van de Beek, O. Edfors and P. O. Borjesson. On channel estimation in OFDM systems. In *Proc. IEEE Vehicular Technology Conf.*, volume 2, pages 815–819, Chicago, IL., July 1995.

[23] P. Schramm H. Asplund J. Medbo, H. Andersson and J. E. Berg. Channel models for hiperlan/2 in different indoor scenarios. Technical report, COST 259 TD(98)070, 1998.

[24] Z. Jianhua and Z. Ping. An improved 2-dimensional pilot-symbols assisted channel estimation in OFDM systems. In *Proc. IEEE Vehicular Technology Conf.*, volume 3, pages 1595–99, Jeju, Korea, Apr. 2003.

[25] J. G. Kemeny and J. L. Snell. *Finite Markov Chains.* Princeton, NJ: Van Nostrand, 1960.

[26] I. Koffman and V. Roman. Broadband wireless access solutions based on ofdm access in ieee 802.16. *EEE Commun. Mag.*, 51(6):96–103, June 2002.

[27] A. F. Kurpiers. Improved channel estimation and demodulation for OFDM on Hf ionospheric channels. In *Proc. IEEE Int'l Conf. HF radio systems and techniques*, volume 1, pages 65–69, Guildford, UK, Jul. 2000.

[28] C. Li and S. Roy. Subspace-based blind channel estimation for ofdm by exploiting virtual carriers. *IEEE Trans. Wireless Commun.*, 2(1), Jan. 2003.

[29] C. Li and S. Roy. Subspace-based blind channel estimation for ofdm by exploiting virtural carriers. *IEEE Trans. Wireless Commun.*, 2(1):141–150, Jan. 2003.

[30] D. Lowe and X. Huang. Adaptive low-complexity MMSe channel estimation for OFDM. In *Proc. ISCIT*, pages 638–643, Sept. 2006.

[31] ITU-R Recommendation M.1225. *Guidelines for evaluation of radio transmission technologies for IMT-2000.* 1997.

[32] H. H. Mmimy. Channel estimation based on coded pilot for OFDM. In *Proc. IEEE Vehic. Tech. Conf.*, volume 3, pages 1375–79, Phoenix, AZ, May 1997.

[33] B. Muquet and M. de Courville. Blind and semi-blind channel identification methods using second order statistics for OFDM systems. In *Proc. SPAWC*, volume 5, pages 170–173, Annapolis, MD, May 1999.

[34] J. J. van de Beek S. K. Wilson O. Edfors, M. Sandell and P. O. Borjesson. Ofdm channel estimation by singular value decomposition. *IEEE Trans. Commun.*, 46(7), July 1998.

[35] M. K. Ozdemir and H. Arslan. Channel estimation for wireless ofdm systems. *IEEE Commun. Surveys Tutorials*, 9(2), 2007.

[36] A. P. Petropulu and R. Zhang. Blind channel estimation for OFDM systems. In *Proc. DSP/SPE, Atlanta, GA*, pages 366–370, Oct. 2002.

[37] J. Proakis. *Digital Communications.* McGraw-Hill, 1989.

[38] J. Ran E. Bolinth R. Grunheid, H. Rohling and R. Kern. Robust channel estimation in wireless LANs for mobile environments. In *Proc. IEEE Vehicular Technology Conf. VTC 2002*, volume 3, pages 1545–1549, Sept. 2002.

[39] M. Ergen S. Coleri and A. Bahai. Channel estimation techniques based on pilot arrangement in ofdm systems. *IEEE Trans. Broadcast.*, 48(3):223–229, Sept. 2002.

[40] B. Muquet S. Zhou and G. B. Giannakis. Subspace-based (semi-) blind channel estimation for block precoded space-time ofdm. *IEEE Trans. Signal Process.*, 50(5):1215–1228, May 2002.

[41] L. L. Scharf. *Statistical Signal Processing: Detection, Estimation, and Time Series Analysis*. Reading, MA: Addison-Wesley, 1991.

[42] Y. Shen and E. Martinez. Channel estimation in ofdm systems. Technical Report AN3059, Freescale Semiconductor, Inc., 2006.

[43] R. Steele. *Mobile Radio Communications*. New York: Wiley, 1974.

[44] P. Strobach. Bi-iteration svd subspace tracking algorithms. *IEEE Trans. Signal Processing*, 45(5):1222–40, May 1996.

[45] L. Tong and S. Perreau. Multichannel blind identification: From subspace to maximum likelihood methods. In *Proc. IEEE*, volume 86, pages 1951–1968, Oct. 1998.

[46] P. Kyritsi A. Molisch D. S. Baum A. Y. Gorokhov C. Oestges Q. Li K. Yu N. Tal B. D. Dijkstra A. Jagannatham C. Lanzl V. J. Rhodes J. Medbo D. Michelson V. Erceg, L. Schumacher and M. Webster. *TGn Channel Models*. May 2004.

[47] K. H. Paik W. G. Jeon and Y. S. Cho. An efficient channel estimation technique for OFDM systems with transmitter diversity. In *Proc. IEEE Int'l. Symp. Personal, Indoor and Mobile Radio Commun.*, volume 2, pages 1246–1250, London, UK, Sept. 2000.

[48] H. S. Wang and P. C. Chang. On verifying the first-order markovian assumption for a rayleigh fading channel model. *IEEE Trans. Vehicular Technol.*, 45(2), May 1996.

[49] J. Wu and W. Wu. A comparative study of robust channel estimations for OFDM system. In *Proc. ICCT*, pages 1932–1935, 2003.

[50] S. Wu and Y. Bar-Ness. OFDM channel estimation in the presence of frequency offset and phase noise. In *Proc. IEEE Int'l. Conf. Commun.*, pages 3366–70, May 2003.

[51] Z. Ding X. Zhuang and A. L. Swindlehurst. A statistical subspace method for blind channel identification in OFDM communications. In *Proc. ICASSP*, volume 5, pages 2493–2496, 2000.

[52] L. J. Cimini Y. Li and N. R. Sollenberger. Robust channel estimation for ofdm systems with rapid dispersive fading channels. *IEEE Trans. Commun.*, 46(7), July 1998.

[53] S. Roy Y. Song and L. A. Akers. Joint blind estimation of channel and data symbols in OFDM. In *Proc. IEEE VTC 2000*, volume 1, pages 46–50, Tokyo, 2000.

[54] R. Zhang. Blind OFDM channel estimation through linear precoding: A subspace approach. In *Proc. 36th Asilomar Conf., Pacific Grove, CA.*, pages 631–633, Nov. 2002.